Research papers

Multiscale analysis of existing actual evapotranspiration products over agropastoral Sahel

Jordi Etchanchu [a],[*], Jérôme Demarty [a], Alain Dezetter [a], Nesrine Farhani [a],
Pape Biteye Thiam [a], Aubin Allies [c],[a], Ansoumana Bodian [b], Gilles Boulet [d],[k],
Nanée Chahinian [a], Lamine Diop [e], Ibrahim Mainassara [a],[f], Pape Malick Ndiaye [b],
Chloé Ollivier [a], Albert Olioso [g], Olivier Roupsard [h],[i],[j]

[a] HSM, Univ. Montpellier, CNRS, IMT, IRD, Montpellier, France
[b] Laboratoire Leïdi "Dynamique des Territoires et Développement", Université Gaston Berger (UGB), Saint Louis, Senegal
[c] GreenTriangle SAS, 10 Rue De La Bourse 75002 Paris 2, France
[d] Centre d'Etudes Spatiales de la BIOsphère (CESBIO), Université de Toulouse, CNRS, CNES, IRD, UT3, INRAE, avenue Édouard Belin, 31400 Toulouse, France
[e] Laboratory of Biological, Agronomic and Food Sciences and Modelling of Complex Systems (LABAAM), Gaston Berger University, Saint Louis BP 234, Senegal
[f] Institut de Recherche pour le Développement (IRD) Representation, 276 avenue de Maradi, Niamey, Niger
[g] Unité de Recherche écologie des Forèt Méditerranéennes (URFM), INRAE, 84000 Avignon, France
[h] Eco&Sols, Univ Montpellier, CIRAD, INRAE, IRD, Montpellier SupAgro, Montpellier, France
[i] CIRAD, UMR Eco & Sols, BP1386, CP18524, Dakar, Senegal
[j] LMI IESOL, Centre IRD-ISRA de Bel Air, BP1386, CP18524, Dakar, Senegal
[k] Indo-French Cell for Water Science, ICWaR, Indian Institute of Science, Bangalore, India

ARTICLE INFO

ABSTRACT

Understanding the spatiotemporal variability of actual evapotranspiration (ET) is a critical issue for better water resources management from plot to basin scale. It is particularly true in the Sahelian region which is very vulnerable in terms of water and agricultural resources, but also very scarcely monitored. This study aims to improve understanding of ET in Sahelian agrosystems by comparing twenty ET products and collections on two areas in Central Senegal and South-Western Niger: Breathing Earth System Simulation (BESS), Derive Optimal Linear Combination Evapotranspiration (DOLCE) v2.1 and v3.0, ERA5 and ERA5-Land, FLUXCOM-RS, Global Land Data Assimilation System (GLDAS) on Noah and Catchment Land Surface Model (CLSM), Global Land Evaporation: the Amsterdam Methodology (GLEAM) v3.5a, v3.5b, v3.6a and v3.6b, Modern-Era Retrospective analysis for Research and Applications v2 (MERRA-2), MODIS Global Evapotranspiration products (MOD16/MYD16), Penman-Monteith Leuning version 2 (PML_V2) v0.1 and v0.1.7, Reliability Ensemble Averaging (REA), Simplified Surface Energy Balance for operational applications (SSEBop) and Water Productivity through Open access of Remotely sensed derived data (WaPOR). In order to assess the abilities and drawbacks of each product, a multi-scale analysis is first performed at local scale with different temporal aggregation levels (daily, decadal, monthly). The best performing products, like GLEAM, MERRA-2 or GLDAS-Noah, have low spatial resolution ($\geq 0.25°$), but shows really good agreement with ET measurements (RMSE ~ 0.5 mm.d^{-1}, R$^2 \geq 0.8$). A multi-scale spatial analysis with different spatial aggregation levels (1, 10 and 25 km) is then performed on interannual composite maps of annual and seasonal ET. Results highlight the different spatiotemporal behaviour of all the products. Products such as ERA5-Land and PML_V2 0.1.7 stand out in this comparison as their higher resolution allows them to describe the spatial patterns of ET realistically and more precisely while having relatively good performances at local scale (RMSE ~ 0.6 mm.d^{-1}, R$^2 \geq 0.7$). Overall, the comparison highlights the need to consider soil moisture to accurately estimate ET in the Sahelian region, as the products considering it generally show better performances. It also points out the lack of a high quality and resolution ET product over the Sahel. Future satellite missions, as well as data fusion techniques, could help to fill up this gap and propose a reference product on Sahelian ecosystems.

* Corresponding author at: 15 avenue Charles Flahault, Hydropolis, CS 14491, 34093 Montpellier cedex 05, France.
E-mail address: jordi.etchanchu@ird.fr (J. Etchanchu).

1. Introduction

Evapotranspiration (ET) is the main component of the Earth surface water budget. It represents around 70 % of precipitation at global scale (Legates and McCabe, 2005; Trenberth et al., 2007; Zhang et al., 2018) and up to 85 % in semi-arid regions (Velluet et al., 2014; Zhang et al., 2018). Given these proportions, estimating ET is of crucial importance for a wide range of applications like water resources management or agricultural production (Labedzki, 2011; Krishna, 2019; Wanniarachchi et al., 2022). It is particularly true in Sahelian regions, which are very vulnerable in terms of water and food supply security (Krishna, 2019). Furthermore, climate change deeply impacts the water cycle. Precipitation in the Sahel shows an increasing trend at annual scale, mainly due to an intensification of the extreme events (New et al., 2006; Panthou et al., 2014; Bodian et al., 2020; Chagnaud et al., 2022). The rain events are less frequent but more intense, generating more runoff (Li et al., 2007; Amogu et al., 2010; Roudier et al., 2014). In addition, the temperature increase generates an increase of potential ET (PET, Ndiaye et al., 2020). However, it is not necessarily the case for actual ET, which seems to decline in semi-arid areas (Pan et al., 2020) due to the change in the precipitation regime and its impact on the land surface and vegetation. Accurately estimating ET is thus critical to understand the interactions between climate and vegetation, and assess the sustainability of the current agricultural systems in semi-arid regions, highly sensitive to water stress and drought occurrence. The lack of in-situ ET measurements in Sahelian region limits our knowledge to the local scale (Cappelaere et al., 2009; Bombelli et al., 2009; Pastorello et al., 2020) and on specific ecosystems (essentially agricultural plots). Yet, knowledge at larger spatial scales is mandatory for the management of water and agricultural resources. Indeed, local information may not be representative of the variety of ecosystems encountered at larger scale that may have different ET tendencies. Moreover, the scarcity of the ET measurement's network in Sahel is not able to capture the spatial variability of eco-climatic conditions that may affect ET estimation at landscape scale (Yuan et al., 2010).

To tackle these issues, nowadays, an increasing number of spatialized ET products have been developed (Liou and Kar, 2014; Zhang K. et al., 2016). There is a wide variety of approach and/or algorithms (Karimi and Bastiaanssen, 2014) that can be classified into three main categories. The first category concerns algorithms based on remote sensing data (Garcia-Santos et al., 2022). Remotely sensed optical and thermal infrared reflectances and products are used to determine ET at satellite overpass, either by solving the surface energy budget or by scaling estimated PET with a stress factor. Continuous series of ET are then produced by using different interpolation methods (Cammalleri et al., 2014; Alfieri et al., 2017; Delogu et al., 2021; Allies et al., 2022) mostly by including other data sources like meteorological reanalysis. The second category uses land surface models (LSM) forced by, or coupled with, meteorological analysis and constrained by assimilated observational data from in-situ measurements and/or satellite acquisitions (Rodell et al., 2004; Simoneaux et al., 2008; Gelaro et al., 2017; Hersbach et al., 2020, Ollivier et al., 2021). It simulates both the surface water and energy budgets, ET being one of the fluxes derived in the process. A third kind of approach uses machine learning methods to upscale in-situ ET measurements with meteorological and remote sensing data. It was first developed at regional scale (Papale and Valentini, 2003; Yang F. et al., 2007) as a sufficiently dense ET measurements network is needed. However, the growth of the FLUXNET eddy-covariance network (Pastorello et al., 2020) has allowed to use such methods at global scale (Jung et al., 2009, 2019) as in the FLUXCOM initiative. Overall, the current literature does not reveal any consensus around an ET product and/or model performing well across all biome types. Moreover, many authors have demonstrated that an ensemble estimation from several models or products generally outperforms any individual product or model (Mueller et al., 2013; Ershadi et al., 2014; McCabe et al., 2016; Michel et al., 2016). These results have encouraged

recent studies to propose a fourth category of algorithms for gridded ET estimations. These algorithms produce synthesis ET estimates based on data fusion of existing gridded ET products (Alemohammad et al., 2017; Hobeichi et al., 2018; Lu et al., 2021).

A number of more or less exhaustive comparisons of the aforementioned ET estimation methods either at global scale (Jimenez et al., 2011; Vinukollu et al., 2011a, 2011b; McCabe et al., 2016) or at regional scale (Hu et al., 2015; Bai and Liu, 2018; Weerasinghe et al., 2020; Chao et al., 2021) are available. Global studies highlight the wide range of estimations provided by the numerous ET products existing. Differences between products range from 10 to 40 mm.month^{-1} at global scale (Jimenez et al., 2011; Vinukollu et al., 2011a, 2011b; McCabe et al., 2016), representing around 30 % relative error compared to mean global ET. These studies also agree that the discrepancies between products increases both at low latitudes and during the hotter seasons, where PET is higher. Regional scale studies (Hu et al., 2015; Bai and Liu, 2018; Weerasinghe et al., 2020; Chao et al., 2021) confirm these conclusions, with similar quantitative results over Europe, CONUS, China and Africa. It also emphasizes that the best products often differ between eco-climatic regions, depending on their inputs and the specificities of each algorithm, with no worldwide consensus. Therefore, reference products need to be determined for each region. Moreover, to evaluate the products' abilities to handle the wide range of applications and scientific issues related to ET from plot to landscape scale, products should be evaluated at different spatial and temporal scale. Indeed, products considered as well performing on specific ecoclimatic regions can be unfit for specific applications due to their spatiotemporal characteristics. However, very few studies evaluate ET products through multi-scale analysis (Cawse-Nicholson et al, 2021). Very few studies are devoted to Sahelian regions (Andam-Akorful et al., 2014; Adeyeri and Ishola, 2021, Allies et al., 2022; Guzinski et al., 2023) and only a low number of ET products have been used. The products were also compared only either at local scale or at a very integrated scale (>50 km) in these studies. Added to the scarcity of in-situ measurements, it contributes to keep the Sahel as one of the regions where the response to climate evolution and land cover changes is the most poorly captured (Marshall et al., 2012; Zhang K. et al., 2015; Zhang X. et al., 2016). Therefore, there is a need to extensively compare ET estimates in West-African ecosystems in order to reliably assess climate and land surface changes effects on the hydrological cycle.

It is particularly true in agrosystems, where the evolution of practices is on the frontline to tackle water and food security issues. Indeed, many concerns arise about the sustainability of the needed agricultural intensification (Keatinge et al., 2001; Jayne et al., 2019). In this context, the impact of agricultural practices on surface fluxes is more and more studied. For example, agroforestry commonly appears to be a great option in systems where subsidence farming is dominant (Droppelmann et al., 2017; Kuyah et al., 2021), both in terms of crop yields and climate change mitigation. However, the current studies over West-Africa mainly focus on yields (Bado et al., 2021) and carbon sequestration (Tschora & Cherubini, 2020) at local scale. Soil practices like tillage or bench terracing are also increasingly used in Sahelian agrosystems to limit soil erosion and improve the infiltration of water in the soil (Maisharou et al., 2015). Agroforestry as well as soil practices are expected to limit direct evaporation from the soil, to the profit of crop transpiration. It could thus locally affect ET, either with higher ET rates during the crop season or with a longer ET cycle. However, the actual impact of such practices' development on water and energy cycle remains poorly documented (Rhoades, 1995; Siriri et al, 2012), especially at larger scale. Gridded ET products can help monitor the effect of the generalisation of such practices on surface fluxes and its impact on water cycle and crop productivity. It could help conclude on whether these practices would be sustainable in regions highly dependent on subsidence farming, such as the Sahel, in a context of climate change.

The present study thus aims at bringing a fuller and actualized overview of existing ET products over Sahel and their abilities to tackle

scientific and societal issues inherent to Sahelian agroecosystems from plot to landscape scale. Twenty gridded ET products from all the aforementioned categories are evaluated over two typical Sahelian agropastoral areas in Central Senegal and Niger and recommendation on their potential applications is proposed. The evaluation is firstly performed at pixel scale against eddy-covariance measurements of ET in typical agropastoral plots. Then a mesoscale analysis over the areas (~130x130km) is performed. As the products present a wide range of spatial and temporal resolutions, they are analysed at different spatial and temporal aggregation levels. Given its greater variety of ecosystems, the focus is done in this study on the Central Senegal area while the Niger area helps supporting the generalizability of the conclusions. It allows to emphasize products which describes well the main ET signal components and those which describe well the spatiotemporal variations. Thus, the discrepancies and uncertainties of the ET products over West Africa are highlighted.

2. Study area

The first study area is a 130x130km zone (13.8°N-17.1°W/15°N-15.9°W) located in the Central-Western part of Senegal (Fig. 1). It is characterized by a semi-arid climate with a rainfall gradient from the North-East to the South-West linked to the oscillations of the West-African Monsoon. Precipitation occurs during a unimodal rainy season spanning from June to September, with annual rates ranging from 450 to 800 mm (Diop et al., 2016). The mean annual minimal and maximal temperatures are respectively around 20 °C and 37 °C (1981–2020 mean at Fatick). The topography is relatively flat as the highest point of the study area is only 137 m Above Mean Sea Level (AMSL). The area is located in Senegal's Groundnut Basin which is one of the main agropastoral regions of the country. Croplands constitute the main land cover type (Fig. 2.a, cf. section 3.2.2) while the natural ecosystems are mainly shrubby and herbaceous savannah. The main crop types are groundnut, millet, sorghum, cowpea and watermelon. Most of the croplands are scattered with trees like baobabs (*Adansonia digitate L.*) or acacias (*Faidherbia albida (Delile) A. Chev.*). Agroforestry is thus common in the area. A flux tower, that monitor hydrometeorological variables at the plot scale, including ET, is located near the city of Niakhar (cf.

section 3.3.1). The area also includes the Saloum river delta, which is home to mangrove forests that protect a unique biodiversity.

The second study area is 175x145km (12.85°N-1.55°E/14.15°N-3.15°E) and located in the South-Western part of Niger, around the capital Niamey (Fig. 1). The rainfall regime is similar to the Central Senegal area but with a mean annual rainfall ranging from 470 mm to 570 mm from South to North. The topography is also relatively flat, ranging from 177 to 274 m AMSL. The area is crossed by the Niger river, draining the plateau area in the South-West, while the Eastern part of the area is mostly endoreic. The plateau zones have very degraded soils with bare soils and seasonal herbaceous vegetation while the rest of the area is a typical Nigerian agropastoral area (Fig. 2.b) with an alternance of rainfed millet crops and shrubby savannah (*Guiera Senegalensis*), forming the main rotation system. A minority of vegetable farming areas are also located on the banks of the Niger river. The area is historically monitored in the frame of the French Observatory of African Monsoon (AMMA-CATCH). Therefore, a flux measurement site is installed near the village of Wankama to monitor the rotation system (cf. section 3.3.2).

3. Data

3.1. Evapotranspiration products

In this study, twenty products and collections are considered, namely BESS, GLEAM 3.5a, 3.5b, 3.6a and 3.6b, MOD16A2v061, MYD16A2v061, PML_V2 0.1 and 0.1.7, SSEBop, WaPOR, ERA5, ERA5-Land, GLDAS-Noah, GLDAS-CLSM, MERRA-2, FLUXCOM RS, DOLCE v2.1 and v3.0, and REA. All algorithm categories previously mentioned are represented, with a wide variety of working principles, versions, spatiotemporal features and time availability (Table 1). A detailed description of the products can be found in appendix A.

3.2. Additional gridded data

To analyse the spatial patterns of the ET products, they were visually compared with a gridded precipitation and a land cover dataset in this study.
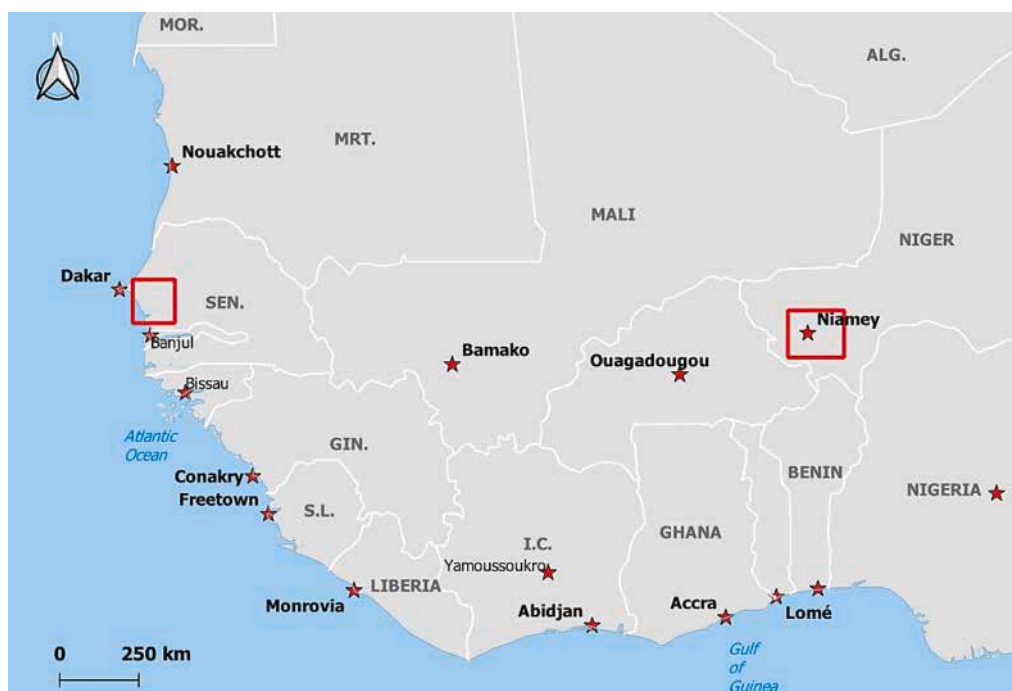

Fig. 1. Location of the study areas (Sources: Natural Earth/GeoSenegal).
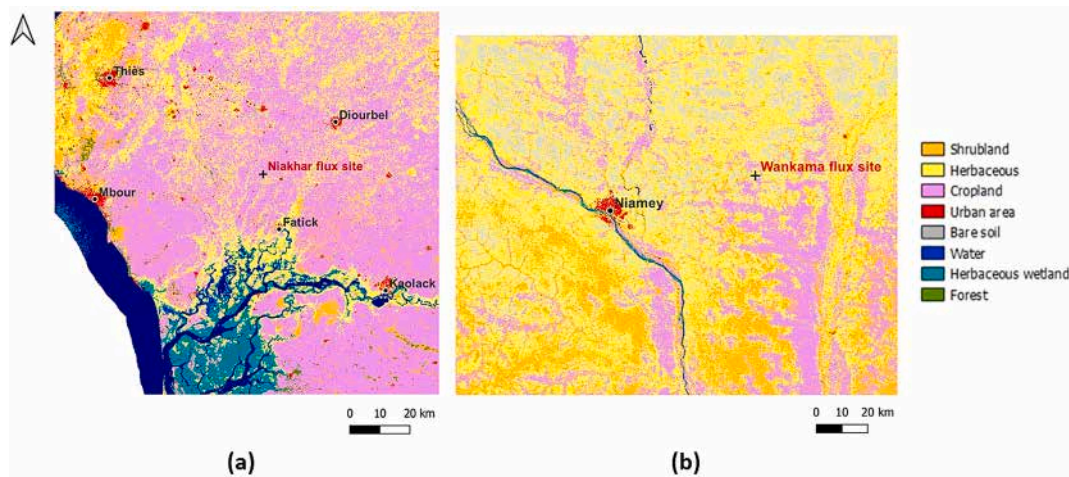
Fig. 2. Land cover map of the Central Senegal (a) and Niger (b) areas in 2018 (Theia OSO).

Table 1

Main features of the evapotranspiration products.

Category	Product Name	Algorithm principle	Spatiotemporal features	Time period	Reference
Remote sensing	BESS	Radiative transfer with photosynthesis & canopy conductance models. ET is then derived by the Penman-Monteith equation.	Global 8-days / 1 km	2000–2015	Ryu et al., 2011; Jiang et Ryu., 2016
	GLEAM v3.5a GLEAM v3.5b GLEAM v3.6a GLEAM v3.6b	Priestley-Taylor formulation with a stress factor based on soil moisture and vegetation water content	Global Daily / 0.25° x 0.25°	1980–2021 2003–2021 1980-present 2003-present	Miralles et al., 2011; Martens et al., 2017
	MOD16A2v061 MYD16A2v061	Penman-Monteith formulation with biome-specific canopy conductance model.	Global 8-days / 500 m x 500 m	2001-present	Mu et al., 2007, 2011
	PML_V2 0.1	Penman-Monteith formulation with Leuning surface conductance model	Global 8-days / 0.05°x 0.05°	2002–2019	Zhang Y. et al., 2010, 2016, 2019
	PML_V2 0.1.7		8-days / 500 m x 500 m	2000–2020	
	SSEBop	ET from ET_0 scaled with evaporative fraction derived from per-pixel land surface temperature and air temperature	Global 10-days / 1 km x 1 km	2000–2015	Senay et al., 2013
	WaPOR	Penman-Monteith formulation with soil and canopy resistances controlled by land surface temperature	Africa 10-days / 250 m x 250 m	2009-present	FAO, 2020
Climate Reanalysis: Global Circulation Model + Land Surface Model	ERA5	Assimilation of satellite- and ground-based observational data in a Global Circulation Model with a Land Surface component	Global Hourly / 0.25° x 0.25°	1950-present	Hersbach et al., 2020, 2023
	ERA5-Land		Hourly / 0.1° x 0.1°		Muñoz-Sabater et al., 2019, 2021
	GLDAS-Noah	Assimilation of satellite- and ground-based observational data in LSMs	Global 3-hours / 0.25° x 0.25°	2000-present	Rodell et al., 2004Beaudoing and Rodell, 2020
	GLDAS-CLSM		1-day / 0.25° x 0.25°	2003-present	
	MERRA-2	Assimilation of satellite- and ground-based observational data in a Global Circulation Model with a Land Surface component	Global Hourly / 0.5°x0.625°	1980-present	GMAO, 2015; Gelaro et al., 2017
Machine-learning	FLUXCOM RS	Median of ensemble estimates from 9 machine-learning algorithms using only remote sensing data as predictors and flux tower data acquired on 224 FLUXNET sites as training dataset	Global 8-days / 0.0833° x 0.0833°	2000–2015	Jung et al., 2019, 2020
Data fusion	DOLCE v2.1 DOLCE v3.0	Linear combination of existing gridded ET products minimizing root mean square error against flux measurements from different flux tower networks	Global Monthly / 0.25° x 0.25°	1980–2018	Hobeichi, 2020 Hobeichi, 2021
	REA	Weighted average of 3 existing gridded product using a reliability ensemble averaging method.	Global Daily / 0.25° x 0.25°	1980–2017	Lu et al., 2021

3.2.1. Climate Hazard group InfraRed precipitation with station data (CHIRPS)

CHIRPS (Funk et al., 2015) is a global gridded precipitation product with a 0.05° spatial resolution and daily to monthly temporal resolution. It provides data from 1981 to now. The algorithm of CHIRPS relies on three main components: i) a gridded climatology of precipitations based

on a spatialization method of meteorological stations climatology (CHPclim), ii) a satellite-only estimation of precipitation based on cloud temperature estimates to derive precipitation duration and intensity (CHIRP), and iii) a blending procedure to include meteorological station data. We chose to use CHIRPS data to analyse the spatial patterns of precipitation as it is proven to be one of the best products over West Africa in the literature, especially at monthly to annual scale (Dembélé and Zwart, 2016; Poméon et al., 2017; Obahoundje et al., 2020; Satgé et al., 2020). CHIRPS annual precipitation spatial patterns are thus used to study the annual evapotranspiration spatial patterns.

3.2.2. Theia OSO Land cover map

The Theia OSO Land Cover Map over Sahel (Vincent et al., 2022) provides a land cover classification at 10 m resolution over the year 2018. This land cover map is produced with the IOTA2 (Inglada et al., 2015) supervised classification algorithm on Sentinel-2 images. As there are very few reference data at Sahelian scale, the algorithm training was performed on the Copernicus Global Land Service Land Cover maps (Buchhorn et al., 2020). The land cover is thus divided in 24 classes. As for the precipitation product, land cover map is used to analyse the spatial patterns of annual and seasonal evapotranspiration.

3.3. Local flux site observations

3.3.1. Niakhar flux site (Senegal)

Data acquired on the "Faidherbia-flux" ecohydrological observatory (https://lped.info/wikiObsSN/?Faidherbia-Flux, data available at FLUXNET ID: SN-Nkr or https://bd.amma-catch.org/main.jsf) located near the village of Niakhar (14.4958°N-16.4536°W) are used in this study. It aims at proposing a long-term survey of a semi-arid agro-silvo-pastoral ecosystem, in terms of productivity, ecosystem services, greenhouse gases fluxes and plant and practices adaptation, in link with the climate evolution (Roupsard et al., 2020; Siegwart et al., 2023). The ecosystem monitored is a typical cropland under acacia trees (*Faidherbia albida (Delile) A. Chev.*). Two eddy-covariance measurements are implemented at different levels (4.5 and 20 m) to dissociate the whole ecosystem behaviour from the crop underneath (Diongue et al., 2022). It estimates the energy and carbon turbulent fluxes, including the ET, with a LI-COR LI-7500 gas analyser combined to a GILL WindMaster 3D sonic anemometer. In this study, we used the 20 m level as it is the most integrated level and thus the most representative of the integration level of gridded ET products. The quality of the measurements is good as the mean annual energy budget closure is 0.94. As it is only possible to compare continuous ET products to in-situ measurements with continuous timeseries, a gap-filled timeseries of ET was used. The gap-filling method used is the one implemented in the REddyProc R package (Wutzler et al, 2018). It is based on look-up tables linking meteorological variables to ET on available periods. The principle is to gather ET fluxes with similar meteorological conditions into separate meteorological classes. Gaps are then filled by determining each gap's meteorological conditions and attribute the ET mean of the corresponding class. However, the gap rate in the Niakhar timeseries is reasonable (<35 % after filtering).

3.3.2. Wankama flux site (Niger)

The Wankama flux site (13.6440°N-2.6299°E) data are gathered since 2005 in the frame of the AMMA-CATCH observatory (https://amma-catch.osug.fr/). It aims for a long term monitoring the millet-shrubby savannah rotation system typical of the Nigerian agropastoral areas (Velluet et al., 2014). Two eddy-covariance systems are implemented on two plots with opposite crop rotations. Both measures turbulent fluxes half-hourly, including ET, with a LI-COR LI-7500 gas analyser combined to a Campbell Scientific CSAT-3 sonic anemometer at 5 m above ground. The ET data cover the 2005–2018 time period. The mean between both plots have been used for the study as they are tens of meters away from each other. The consequent gap rate in ET timeseries

is around 13 %. As no gap-filled data is proposed on this station, we only used complete days, leading to around 17 % missing days. The mean annual energy budget closure is acceptable, at 1.1 over millet and 1.25 on the fallow plot.

4. Methods

4.1. Uniformization of products spatio-temporal characteristics

The large variety of spatial and temporal resolution of the products, added to the fact that their original grids are not necessarily aligned, is a challenge to perform direct cross-comparison. Choosing a single spatial and temporal resolution for the comparison would be unfair either for low-resolution products (in the case of high-resolution comparison) or high-resolution products (in case of low-resolution comparison). Best option is then to use different aggregation levels for the comparison, including in each level only products with higher resolution. For example, for a 10 km aggregation scale, only products with a spatial resolution higher or equal to 10 km would be considered, whereas a 25 km aggregation scale would additionally include products with resolutions between 10 and 25 km. Common practice in this case is to first resample all the products on a reference high-resolution grid with the nearest neighbour method in order to keep the resampled products as close as possible to the original products. Then resampled products are aggregated at the different levels defined previously. This general methodology is illustrated in Fig. 3. A similar approach should be adopted to cope with the different temporal resolutions (Fig. 4) by first resampling the values at high temporal resolution, using previous, next or nearest neighbouring value, depending on the product's original time format, i.e. if its values are representative respectively of the next, the past or the surrounding time period of the given date. In both cases, best practice is then to only compare the products with native resolutions higher or equal to the aggregation levels considered. In our study, the ET products are resampled at 1 km/daily resolutions, assuming this spatiotemporal scale is a good compromise for agricultural or small basin hydrology issues. The target kilometric grid chosen is the MODIS 1 km grid. Native products with a lower resolution (>=1km) are thus resampled using the nearest neighbour approach as described previously. Products with a higher resolution (<1km) but aligned with the MODIS 1 km grid (PML_V2 0.1.7, MOD16/MYD16) are resampled with bilinear resampling, allowing for an arithmetic averaging of the four pixels present in a 1 km pixel. Only WAPOR have both a higher resolution (500 m) and a grid that is not aligned with MODIS. In this particular case, a calculation of the covering portion of each native resolution pixel on the 1 km pixel is used and a weighted average based on these portions is performed (Eq. (1).

$$ET_{1km} = \sum_{i=1}^{n} \frac{surf_i \times ET_i}{\sum_{i=1}^{n} surf_i} \tag{1}$$

"n" represents the number of native pixels having a value (to exclude masked areas of the calculation) that partially or entirely covers a 1 km pixel, "$surf_i$" the covering surface of the native pixel "i" on the 1 km pixel and ET_i the ET value of the native pixel "i". These methods allow for a comparison of all the products without altering the native information they contain with the use of more complex aggregation or disaggregation methods, which often use external data to recreate an artificial spatial variation.

The temporal resampling to daily resolution is then performed. Native products with infra-daily temporal resolution (GLDAS-Noah, ERA5, ERA5-Land, MERRA-2) are summed over the day. On the other products, with lower temporal resolution, the mean daily ET value over their native timestep is first computed, when not provided. This value is then duplicated each day within the timestep. The unit of all ET products is finally harmonized to mm.d^{-1}.
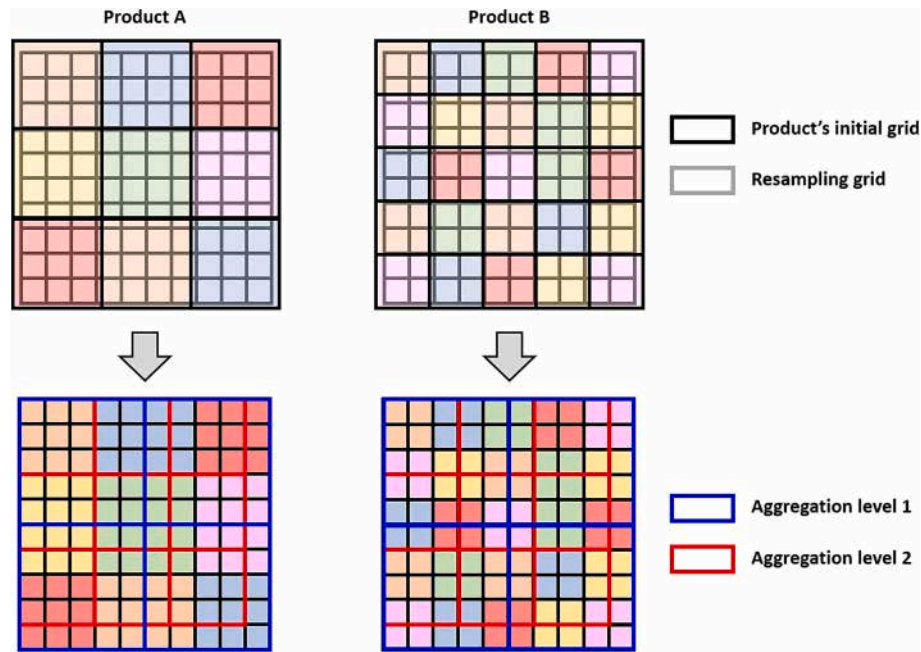
Fig. 3. Illustration of the resampling and aggregation steps for two products with different spatial grids and two aggregation levels. In this case, both products should be compared at aggregation level 1 whereas only product B should be compared at aggregation level 2.
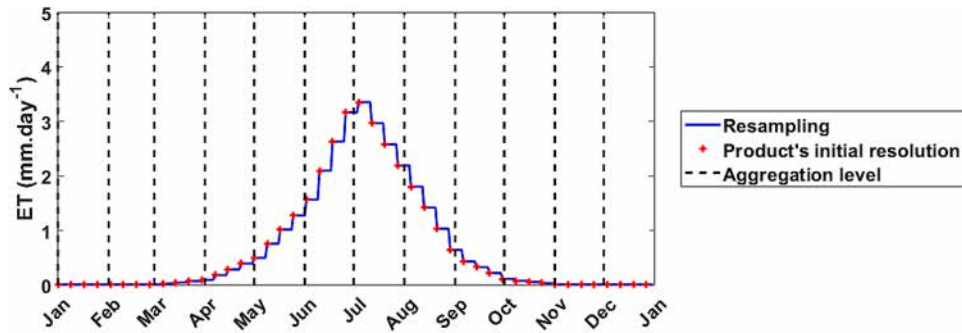

Fig. 4. Illustration of the temporal resampling and aggregation steps. In this example, an 8-day resolution product is first resampled daily and then monthly aggregated.

4.2. Products comparison at station scale

Products are first evaluated with observations acquired on the Niakhar and Wankama flux stations. To this end, the pixel including each station is extracted for each product. To check the capabilities of the products to reproduce observed seasonality and interannual variability on available measurements period, interannual average of the daily ET of each product and of the observations is computed over the ET measurement period on both sites. Moreover, resampled ET products and observations are also temporally aggregated at daily, decadal and monthly scales to perform multi-scale temporal analysis. At each aggregation scale, only products with a native temporal resolution higher or equal to the aggregation level are considered for comparison. Finally, three statistical scores between each product and the observations are computed at each aggregation level: the bias, the correlation coefficient R^2 and the Root-Mean Square Error (RMSE). RMSE and bias are also calculated separately for both the dry (January-February-March) and wet (July-August-September) seasons.

4.3. Spatialized intercomparison

The capabilities of each product to represent the spatial patterns of ET, according to the landscape features, are evaluated through a multi-scale spatial comparison. Three spatial aggregation levels are considered: 1 km, 10 km and 25 km. Only the products with higher or equal native spatial resolution are considered in each case. These aggregation levels were chosen because they are representative of three main groups of products in terms of spatial resolution. Each group has specific intended applications, respectively agriculture and small basin hydrology, region scale meteorology and large basin hydrology, and global climatological studies. Then, for both study areas, the mean annual ET, as well as the mean seasonal ET over the dry season (January, February, March) and the rainy season (July, August, September), are computed over the common period of all the products (2009–2015) for every aggregation level. A statistical cross comparison of the products is also performed by comparing the medians and the Pearson correlation coefficient (Eq. (2) between their spatial distributions at both yearly and seasonal temporal aggregation scales.

$$r = \frac{\sum_{j=1}^{m}(ET_1(j) - \overline{ET_1})(ET_2(j) - \overline{ET_2})}{\sqrt{\sum_{j=1}^{m}(ET_1(j) - \overline{ET_1})^2}\sqrt{\sum_{j=1}^{m}(ET_2(j) - \overline{ET_2})^2}} \tag{2}$$

"m" represents the number of pixels with values in the map, "j" the jth

pixel in the map (conserving the order of the pixels within the map), "ET₁" the first ET product to be compared and "ET₂" the second one. "$\overline{ET_i}$" is the spatial mean of product "i" over the entire map.

5. Results

5.1. Local comparison

To illustrate the temporal behaviour of each product, the interannual daily ET cycle of the products over the measurement period (2018–2021) at the Niakhar flux station are compared in Fig. 5.
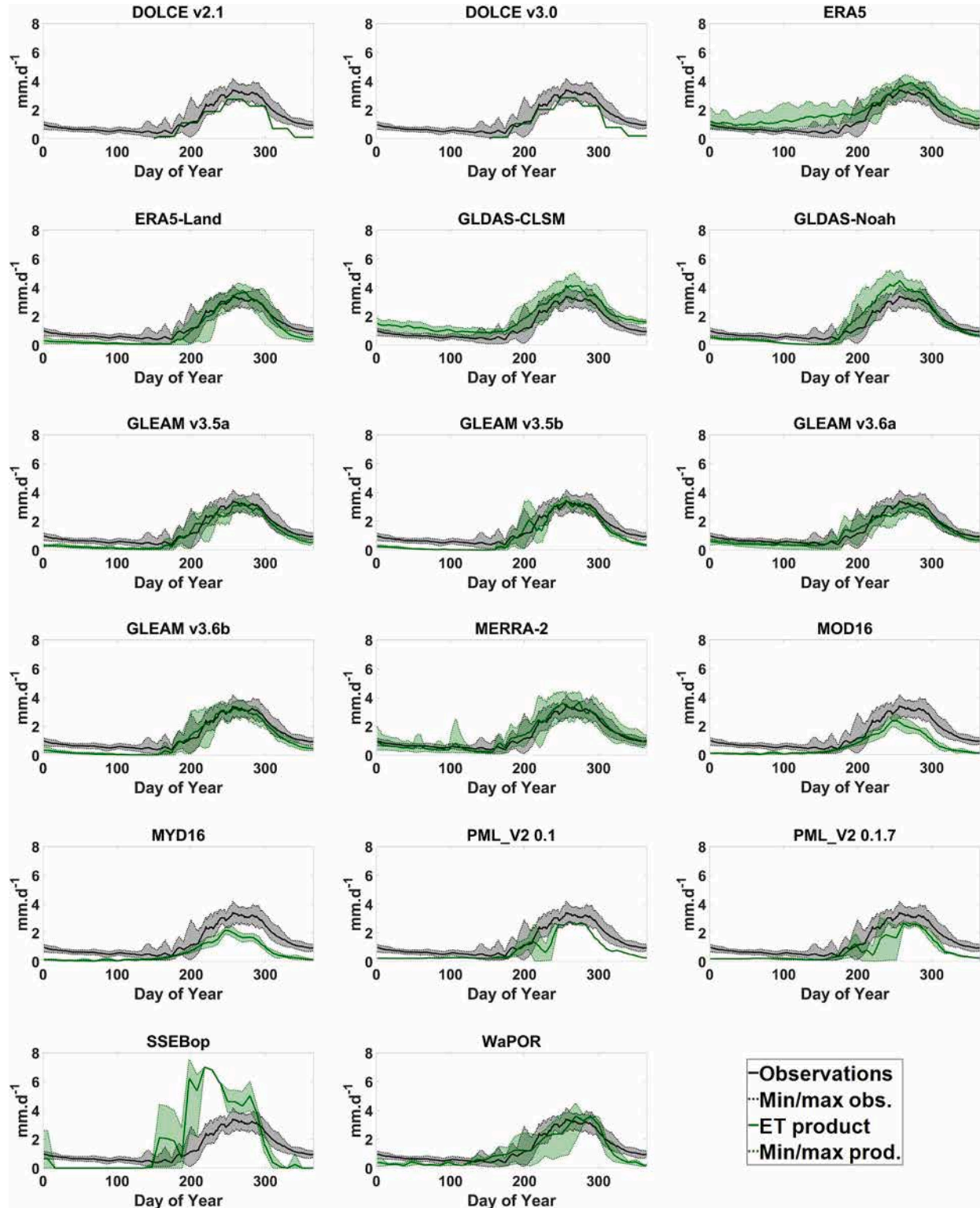

Fig. 5. Interannual (2018–2021) daily ET cycle at the Niakhar flux station, smoothed with a 10-days moving mean. Shaded areas represent the interannual minimal-maximal values for each day.

Complete timeseries are presented in appendix B. BESS, FLUXCOM RS and REA are not represented due to the disjunction between their timespans and the measurement period. Also, DOLCE products have no interannual variability represented because only a single year is available in this period. As the measurements begin at the start of the wet season, scores during dry season are not available for these two products. PML_V2 0.1 product also has no interannual variability on the year's second half, because only a year and a half is available in the measurements period. The statistical scores of the products compared to measurements at the different temporal aggregation levels are summarized in Fig. 6.

Highly biased products (ERA5, GLDAS-CLSM, MOD16, MYD16, PML_V2 0.1.7, SSEBop) are clearly identified in Fig. 6, with absolute biases between 0.5 and 0.8 mm.d^{-1}. ERA5 and GLDAS-CLSM exhibit a permanent positive bias. On one hand, the bias is pretty constant for GLDAS-CLSM (Fig. 5), allowing it to describe well ET seasonality, which is confirmed by R^2 over 0.7. Moreover, its interannual variability is comparable to the measurements. On the other hand, ERA5 only has a good representation of ET during the peak of the rainy season until the beginning of the dry season. Then ET is increasingly overestimated across the dry season. It translates into a drop of the performances with R^2 around 0.6 and RMSE around 1 mm.d^{-1}. Its interannual variability is also high during dry season. For negatively biased products, MOD16 and MYD16 have the largest bias of all products at annual scale ($\sim$0.8 mm.d^{-1}) but seemingly proportional to ET. They thus represent quite well the temporality of the ET cycle, with R^2 over 0.7. Their interannual variability is however small. PML_V2 0.1 and 0.1.7 exhibit about the same bias behaviour, in smaller proportions (respectively $\sim$ 0.3 and $\sim$ 0.7 mm.d^{-1}). It is worthy to note that, despite only having respectively one and a half and two years in common with the measurement period, the interannual variability in early wet season is high, especially for PML_V2 0.1.7. Another point that stands out about the PML products is that they have the greatest degradation of the scores through temporal resolution increase out of all products, especially for PML_V2 0.1. The temporality of ET is the most impacted, with a drop of R^2 of about 0.2.

Fig. 6 also highlights that SSEBop has seasonality problems, with R^2 under 0.4. The amplitude of the proposed ET cycle is too high, with daily ET rates over 6 mm.d^{-1} in the heart of the wet season, causing bias just under 3 mm.d^{-1} during this season. The seasonality is also advanced by about a month compared to the measurements, be it on the rise or the drop of ET. During dry season, ET is equal to 0 mm.d^{-1} during months every year, without interannual variations. It translates into a 0.6 mm.d^{-1} bias during dry season. This behaviour shows that SSEBop seems highly sensitive to the near-surface soil hydric state, despite having no representation of soil moisture in its algorithm.

Best performing products appears to be the GLEAM products, GLDAS-Noah, MERRA-2 and the DOLCE products, closely followed by ERA5-Land, with R^2 above 0.8, limited bias ($<$0.4 mm.d^{-1}) and RMSE ($<$0.5 mm.d^{-1}). WaPOR is the runner up, not showing the best scores but being the best within the products that have an under-kilometric spatial resolution. Both DOLCE products represent quite well the seasonality of the ET cycle, despite their monthly resolution. However, they present a noticeable underestimation in the transition from wet to dry season. GLDAS-Noah capture well the ET seasonality. The interannual variability is also comparable to the measurements. However, GLDAS-Noah shows an overestimation during the wet season, with a bias around 1 mm.d^{-1}. ERA5-Land exhibits good performances on ET during the entire vegetation cycle (D150-D320) but a slight underestimation during the dry period. GLEAM products seem to be the closest ones to the measurements, especially during wet season. Particularly, GLEAMa products show better behaviour than GLEAMb products in the transition from wet to dry season. The interannual variability seems comparable to the measurements except at the end of the wet season. Indeed, GLEAM products tend to have lower interannual variability in the drop of the ET cycle than the measured ET. MERRA-2 presents performances on par with GLEAM at annual scale, having slightly lower performances during

wet season but compensating it with the best representation of ET dynamics during transition from wet to dry season and during dry season, exhibiting bias under 0.6 mm.d^{-1} in this latter. Its interannual variability is however higher than the measurements during wet season. MERRA-2 also shows signs of typical out-of-season rainfall events around D100 which is not present in the measurements, illustrating the mismatch between flux tower scale and MERRA-2 low spatial resolution. Moreover, the degradation of its scores when going from decadal to daily resolution is slightly higher than other products, apart from PML_V2 products. Finally, WaPOR shows a good timing of the ET cycle but with a slight delay in the peak timing and a steeper decrease of the cycle. ET is then underestimated in early dry season. The interannual variability during the rise of the ET cycle is also greatly overestimated. It is interesting to note that, while DOLCE products only provide monthly resolution, the other aforementioned products have limited degradation of their scores ($<$0.1) through the increase of temporal resolution, even when reaching the daily scale (Fig. 6).

Table 2 shows the same statistical scores as Fig. 6 but on the Wankama flux station. It shows that ET products have mostly very similar behaviours on both sites. GLEAM products and GLDAS-Noah remain the best performing products at all temporal scales. However, the overestimation of GLDAS-Noah seen on the Niakhar flux site is still observable with bias up to 0.4 mm.d^{-1} in wet season, leading to higher RMSE than GLEAM products. MERRA-2, ERA5-Land and the two DOLCE products are the runner ups, despite having large negative biases during wet season ($\sim$ 0.6 mm.d^{-1}) for the three latter. GLDAS-CLSM and ERA5 still have positive bias, especially during dry season ($>$0.5 mm.d^{-1}). However, unlike on the Niakhar site, their bias is largely negative ($\sim$0.5 mm.d^{-1}), leading to a drop of correlation ($R^2 \sim$ 0.5, 0.7 and 0.8 at daily, decadal and monthly scale respectively). On the other hand, MOD16/MYD16 still have the largest negative bias (-1.2 mm.d^{-1} overall, -2.7 mm.d^{-1} during wet season). SSEBop displays similar behaviour than on Niakhar, with ET underestimation during dry season and brief peaks of ET during wet season, leading to maximal ET rates of 7 mm.d^{-1} (not shown here). However, the occurence of such peak is lower, leading to a large negative bias during wet season ($>$0.5 mm.d^{-1}), unlike on the Niakhar site. Its R^2 is largely affected, with values between 0.4 and 0.6 across scales. This erratic behaviour also leads SSEBop to have the greatest degradation of its scores across scales. Unsurprisingly, MOD16/MYD16 and SSEBop thus have the largest RMSE ($>$1 mm.d^{-1}). PML_V2 products performs better on the Wankama site than on the Niakhar site when it comes to bias, but with a middling R^2 ($\sim$0.75). The main difference between both sites is the large degradation of performances of WaPOR on the Wankama site compared to the Niakhar site. Indeed, it shows a very different behaviour with large positive bias during dry season ($\sim$0.3 mm.d^{-1}) and negative bias during wet season ($\sim$1 mm.d^{-1}), leading to quite low R^2 ($\sim$0.65) and large RMSE ($\sim$0.8 mm.d^{-1}) at decadal and monthly scale.

5.2. Spatial cross-comparison

To illustrate the spatial cross-comparison, the Senegal area has been chosen, as it has a wider ecosystem diversity and precipitation gradient. Fig. 7 shows the maps of mean annual ET of each product over their common period (2009–2015) over the central Senegal. These maps are also compared to the mean annual precipitation from CHIRPS over the same area and period (Fig. 8). All the products except for three, GLDAS-CLSM, GLDAS-Noah and FLUXCOM-RS, seem to be able to capture the increase in ET rates expected over the mangrove of the Saloum delta (Fig. 2). For GLDAS products, it is hard to conclude because of the 0.25° spatial resolution but they seem to be more influenced by the general precipitation gradient (Fig. 8) than the difference in ecosystem. Indeed, the gradient in ET rates follows a North-West to South-East direction. It is interesting to note that the CHIRPS precipitation product seems influenced by the delta. This effect does not seem to be present in the GLDAS products, either because of the precipitation forcing or because it
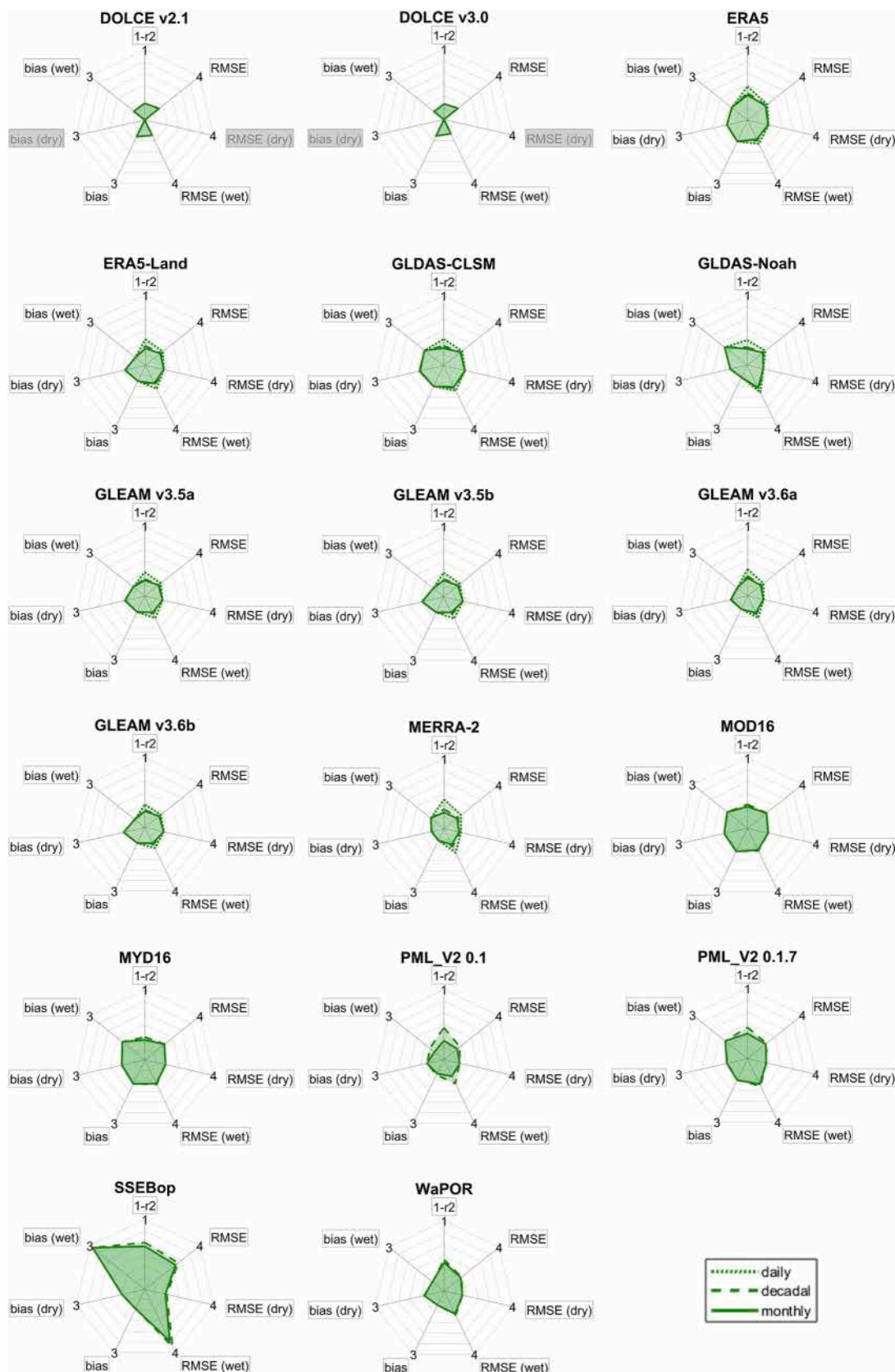
Fig. 6. Statistical scores of the ET products compared to the Niakhar ET measurements at different temporal aggregation scales (day, decade and month). Bias and RMSE are expressed in mm.d^{-1}.

Table 2
Statistical scores of the ET products compared to the Wankama ET measurements at different temporal aggregation scales (day, decade and month). Bias and RMSE are expressed in mm.d^{-1}.

Aggregation level	Daily							Decadal							Monthly						
Product Name	R²	Bias	Bias (dry)	Bias (wet)	RMSE	RMSE (dry)	RMSE (wet)	R²	Bias	Bias (dry)	Bias (wet)	RMSE	RMSE (dry)	RMSE (wet)	R²	Bias	Bias (dry)	Bias (wet)	RMSE	RMSE (dry)	RMSE (wet)
BESS								0.78	-0.45	0.30	-1.31	0.87	0.32	1.37	0.87	-0.52	0.31	-1.25	0.85	0.32	1.28
GLEAM v3.5a	0.68	-0.20	0.01	-0.42	0.77	0.15	1.02	0.87	-0.23	0.02	-0.67	0.51	0.13	0.83	0.91	-0.25	0.01	-0.44	0.44	0.11	0.59
GLEAM v3.5b	0.71	-0.17	0.00	-0.27	0.73	0.16	0.92	0.89	-0.18	0.00	-0.54	0.44	0.12	0.72	0.93	-0.19	-0.01	-0.33	0.37	0.11	0.47
GLEAM v3.6a	0.67	-0.17	0.03	-0.47	0.78	0.21	1.06	0.88	-0.19	0.04	-0.62	0.49	0.18	0.81	0.92	-0.22	0.03	-0.49	0.44	0.16	0.64
GLEAM v3.6b	0.73	-0.20	-0.02	-0.31	0.72	0.14	0.91	0.88	-0.22	-0.01	-0.59	0.47	0.11	0.75	0.93	-0.23	-0.02	-0.36	0.40	0.10	0.49
MOD16A2v061								0.41	-1.21	-0.15	-2.70	1.63	0.16	2.77	0.43	-1.30	-0.15	-2.56	1.69	0.16	2.60
MYD16A2v061								0.41	-1.23	-0.15	-2.71	1.66	0.17	2.77	0.43	-1.34	-0.15	-2.58	1.72	0.16	2.62
PML_V2 0.1								0.72	0.01	0.08	-0.43	0.65	0.12	1.11	0.77	-0.02	0.08	-0.13	0.58	0.11	0.84
PML_V2 0.1.7								0.71	-0.05	0.00	-0.44	0.69	0.07	1.18	0.76	-0.08	0.01	-0.11	0.62	0.06	0.90
SSEBop								0.39	-0.32	-0.14	-0.96	1.29	0.24	2.08	0.56	-0.37	-0.14	-0.51	0.98	0.18	1.29
WaPOR								0.61	-0.18	0.28	-0.38	0.82	0.37	1.14	0.69	-0.24	0.27	-1.07	0.76	0.33	1.20
ERA5	0.55	0.28	0.65	-0.28	0.94	0.72	1.02	0.72	0.25	0.65	-0.65	0.71	0.69	0.69	0.81	0.22	0.64	-0.30	0.62	0.68	0.49
ERA5-Land	0.59	-0.32	-0.06	-0.61	0.92	0.17	1.28	0.74	-0.34	-0.05	-0.53	0.71	0.14	1.01	0.80	-0.35	-0.06	-0.62	0.64	0.11	0.84
GLDAS-Noah	0.66	0.34	0.21	0.37	0.91	0.24	1.14	0.86	0.35	0.22	0.34	0.62	0.24	0.72	0.93	0.37	0.21	0.44	0.51	0.23	0.62
GLDAS-CLSM	0.48	0.18	0.52	-0.55	0.97	0.56	1.27	0.68	0.15	0.53	-0.49	0.71	0.57	0.94	0.71	0.13	0.52	-0.51	0.68	0.55	0.78
MERRA-2	0.60	0.22	0.11	0.02	0.89	0.19	1.10	0.82	0.22	0.11	0.03	0.57	0.17	0.65	0.85	0.23	0.11	0.01	0.52	0.16	0.44
FLUXCOM RS															0.86	-0.12	0.44	-0.53	0.49	0.45	0.65
DOLCE v2.1								0.80	-0.09	0.42		0.58	0.44	0.68	0.84	-0.26	0.05	-0.59	0.56	0.18	0.77
DOLCE v3.0															0.93	-0.44	-0.16	-0.74	0.58	0.18	0.80
REA								0.78	0.20	0.58	-0.44	0.62	0.59	0.73	0.85	0.18	0.57	-0.28	0.55	0.58	0.51

is dampened by the biomes' parameters used in this deltaic area. As for FLUXCOM-RS, ET rates are lower in the delta than in the rest of the area. It is unrealistic for wetland ecosystems where ET is expected to be near potential ET. This behaviour could be explained by the fact that there are no ET observations over tropical mangrove ecosystems in the FLUXNET network. The neural network used in FLUXCOM-RS is thus in an extrapolation case and does not perform well in such case. For the rest of the products, as expected, the ET rates over the delta are higher than on the remaining area, but with very different increases from a product to the other. BESS, DOLCE v2.1 and v3.0, and MOD16/MYD16 show small increases in ET over the delta compared to the agricultural areas, between 100 and 200 mm.yr^{-1}. Conversely, ERA5, ERA5 Land, the different GLEAM versions, MERRA-2, REA and WaPOR show increases ranging from 500 mm.yr^{-1} to 800 mm.yr^{-1} over the delta, which can be deemed as realistic values. Finally, the two versions of PML_V2 and SSEBop show increases around or over 1500 mm.yr^{-1} over the delta. It confirms that SSEBop is highly sensitive to the near-surface hydric state. This is also highlighted by the coastal ET rates. As for PML_V2, ET rates over 2000 mm.yr^{-1} are reported on very specific patches, probably linked to the ecosystem map used to derive the ET algorithm parameterization. ET rates on the delta for both these products are way higher than the annual rainfall and seems more in accordance with potential ET, which should be the case over wetlands.

Apart from the representation of the delta, most of the products show a North-West to South-East ET gradient which agrees with the precipitation gradient (Fig. 8), once again with various levels depending on the products, except BESS and FLUXCOM-RS. These two products show almost no ET gradient and very few changes between ecosystems beside the delta. BESS also has high ET values around masked areas (urban areas, open water). It seems due to a technical problem in the production of ET maps around masked areas. Most of the products also show higher ET rates on the croplands located to the south-east of the delta. This area, besides having higher precipitation, hosts intensive agriculture practices while essentially subsistence farming is practiced in the rest of the study area. Despite being too sensitive to wet conditions, the spatial distribution of SSEBop annual ET rates over the area seems quite good as it clearly highlights the main ecosystems and the precipitation gradient. Concerning the PML_V2 products, the spatial distribution, including the delta, is quite homogeneous over specific areas with a clear delineation between them and very abrupt transitions in-between. PML_V2 0.1.7 even shows this kind of behaviour within the delta, with an erratic spatial distribution.

More specifically, the coastal pixels of DOLCE v3.0, ERA5, GLEAM and MERRA-2 are deeply influenced by the presence of open water, which is realistic but could be a problem for a range of coastal studies (e. g. coastal hydrology and hydrogeology, saline inclusions, coastal agriculture) due to their low spatial resolution. Same problem occurs with low resolution products that uses large margins on coastal areas to avoid mixed sea/land pixels, like GLDAS products.

A quantitative cross comparison of the ET products is then performed by analysing the spatial median of each product on both areas (Fig. 9, Fig. 10) as well as the Pearson correlation coefficients (Fig. 11) on the spatial distributions of the mean annual and seasonal ET over Central Senegal, as described in section 4.3.

The spatial medians (Fig. 9) on Central Senegal allows to identify biases between products without being too influenced by the extreme values. The separation of the results between dry and wet season gives insight about whether the local scale behaviours (Sect. 5.1) of the products between each other are observable at larger scale or not. Therefore, SSEBop's high ET estimates in wet season (50–70 mm. month^{-1}) and low estimates in dry season (5–15 mm.month^{-1}) compared to other products is visible at all aggregation levels. It leads to a general over estimation (100–200 mm.yr^{-1}) compared to the majority of other ET products at annual scale. ERA5, GLDAS-CLSM, MERRA-2 and REA also tend to have higher ET estimates than other products at annual scale (150–500 mm.yr^{-1}). It is particularly due to their positive bias
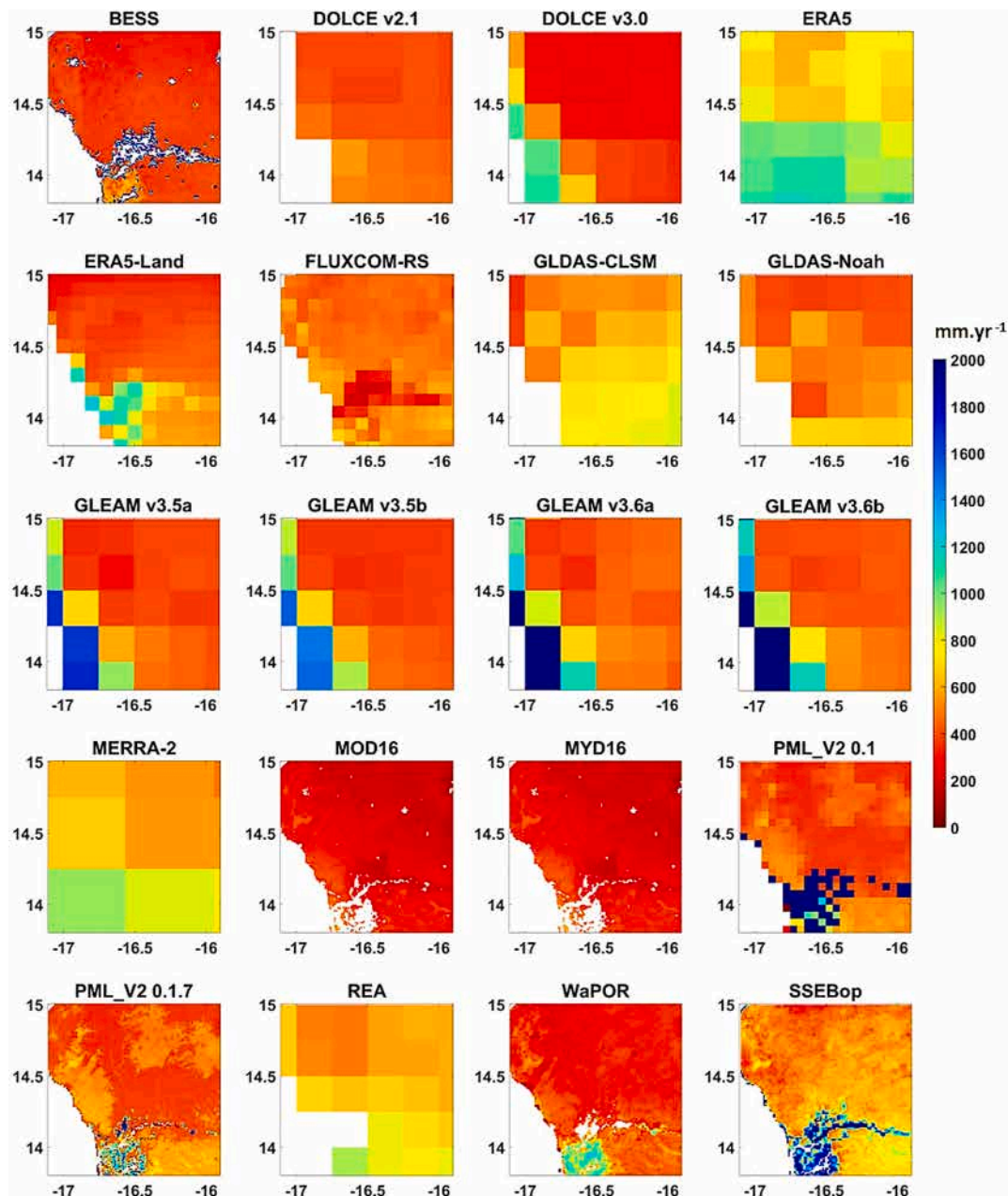
Fig. 7. Mean annual ET (2009–2015) in mm over Central Senegal.

($\sim$20 mm.month^{-1}) in dry season, reproducing the behaviour already seen at local scale. Concerning MERRA-2, the results show a different behaviour than at local scale. On the other side of the spectrum, MOD16/MYD16 tend to have lower ET estimates than other products at all scales and throughout the seasons with median differences ranging from 100 to 500 mm.yr^{-1}. DOLCE v3.0 have such trend too (150–200 mm.yr^{-1}) compared to other product. WaPOR also displays such trend, with similar underestimation throughout the seasons, showing different behaviour compared to other product than at local scale. FLUXCOM-RS is not amongst the highest ET estimates at annual scale compared to other products but, as ERA5, MERRA-2, GLDAS-CLSM and REA, it stands out when it comes to the dry season, with a median difference around 15 mm.month^{-1} compared to other products (besides the four aforementioned). Same goes for BESS, which has middling ET estimates at annual scale but with relatively high estimates compared to other products during dry season (+5–10 mm.month^{-1}). The rest of the products, namely DOLCE v2.1, ERA5-Land, GLDAS-Noah, the GLEAM versions

and the PML_V2 products, all show quite the same median amplitude of annual and seasonal ET, with few differences at all scales. The spatial medians of ET on South-Western Niger (Fig. 10) shows that this area is generally drier than Central Senegal, with lower ET rates, especially during dry season. However, the ET products rank similarly to Central Senegal when it comes to annual ET. Few products show noticeable differences in their behaviour between both areas. For example, MOD16/MYD16 products appears to be too strongly influenced by the dryer conditions on Niger, with extremely low ET rates throughout the year (<50 mm.yr^{-1}). FLUXCOM-RS ET also seems to be on the lower side of the products compared to Central Senegal, despite having one of the highest dry season ET ($\sim$10 mm.month^{-1}). GLDAS-Noah also appears to have higher estimations compared to other products than in Central Senegal, joining the group formed by ERA5, MERRA-2, GLDAS-CLSM, SSEBop and REA. As in Central Senegal, GLDAS-Noah and SSE-Bop wet season ET ($\sim$90 mm.month^{-1}) even if the gap with other products is deeply reduced for SSEBop. As in Central Senegal, ERA5,
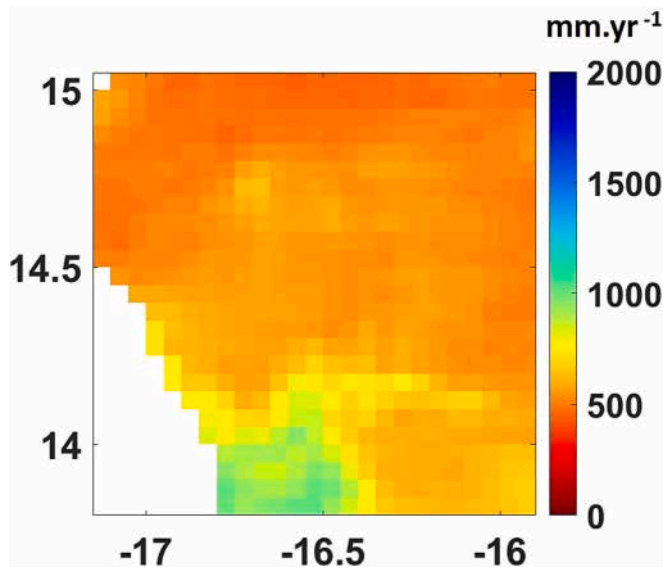
Fig. 8. Mean CHIRPS annual precipitation (2009–2015) in mm over Central Senegal.

GLDAS-CLSM and REA have high dry season ET compared to other products (~15 mm.month^{-1}), explaining their ranking at annual scale. Similarly, BESS and FLUXCOM-RS still have one of the highest ET rates in dry season in South-Western Niger, as well as in Central Senegal. It is compensated at annual scale by their low ET rates during wet season (~40 mm.month^{-1}). WaPOR also seems in this case in South-Western Niger, with the lowest wet season ET rates, although it was not the case in Central Senegal. GLEAM products, PML products and DOLCE

v2.1 shows a good agreement of annual and seasonal ET while DOLCE v3.0 is on the lower side of the products, as in Central Senegal. These spatial results on South-Western Niger also correlates well with the local scores on the Wanakama flux station.

An illustration of spatial patterns analysis on Central Senegal, with the Pearson correlation coefficient, is shown in Fig. 11. It allows to identify the differences between products in the spatial repartition of ET (Fig. 7). Some products stand out in terms of spatial decorrelation with other products. Particularly, FLUXCOM-RS is strongly decorrelated (R<=0) from the other products during the wet season, which is due to the low ET rates produced over the Saloum delta. It leads to a general decorrelation (R≈0.6) at annual scale. Interesting enough, this decorrelation is much stronger (R≈0.2) at smaller aggregation scale (10 km), meaning the finer the spatial resolution is, the less FLUXCOM-RS performs. In a similar way, SSEBop also decorrelates (R≈0.3) during the wet season, throughout the spatial scales. The analysis of the interannual maps of wet season ET (not shown in this paper) confirms the high sensibility of SSEBop to the rain patterns, leading to a quite realistic spatial distributions but with very high ET rates and strong contrasts between zones, which affects the Pearson correlation coefficient calculation. However, during the dry season, and consequently at yearly scale, its spatial distribution seems quite similar, leading to a small decorrelation overall. Nonetheless, it should be noted that the decorrelation of SSEBop with respect to the other products becomes stronger with the improvement of the spatial resolution. GLDAS-CLSM has a slight decorrelation (R≈0.5) during the wet season but a stronger one during the dry season (R≈0.3), leading to an overall decorrelation at annual scale (R≈0.5). This may be explained by the fact that GLDAS-CLSM does not seem to capture the Saloum delta effect on ET. Therefore, there is a strong decorrelation in dry season compared to other products which capture it. It confirms the analysis highlighted in Fig. 7. Finally, BESS shows large scale decorrelation compared to the other
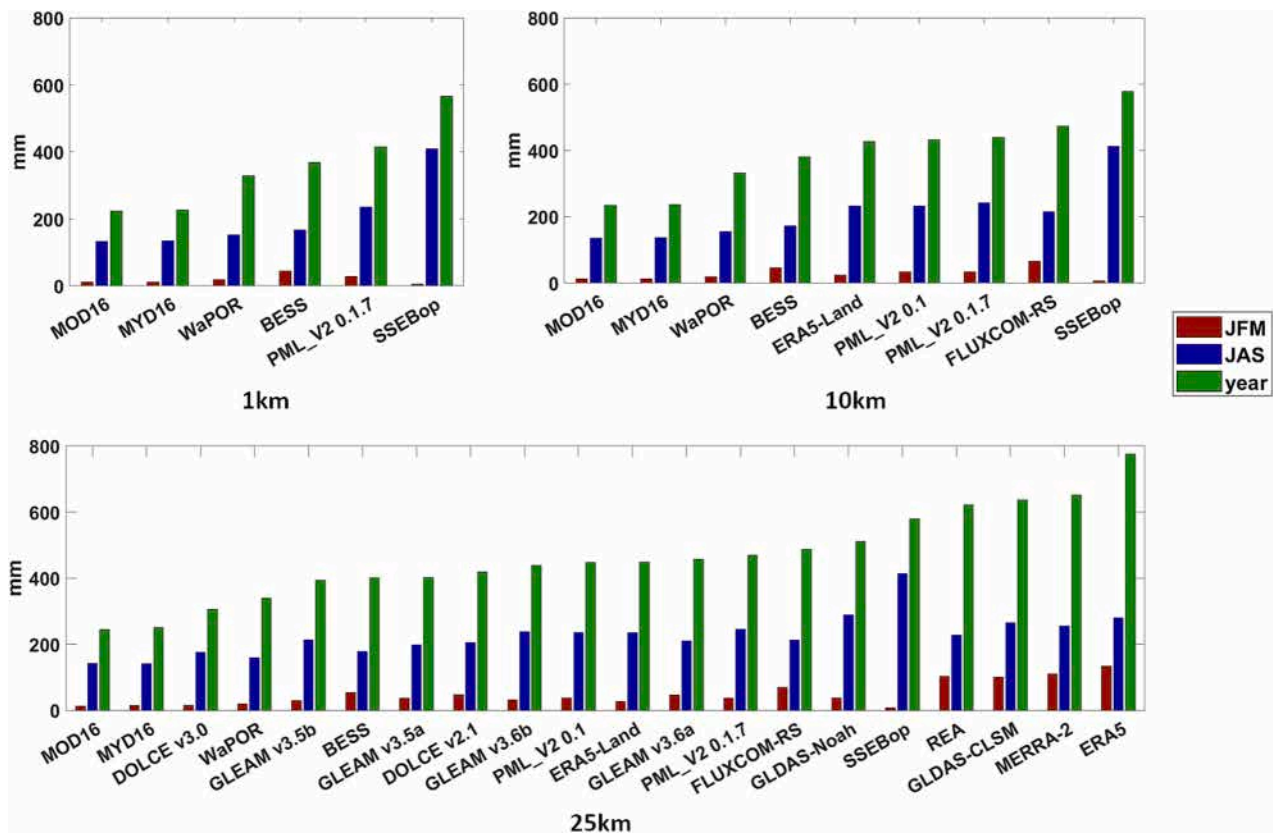

Fig. 9. Median of each product's spatial distribution on mean (2009–2015) annual and seasonal ET over dry (January to March) and wet (July to September) seasons over Central Senegal at different spatial aggregation levels: 1 km (a), 10 km (b), 25 km (c).
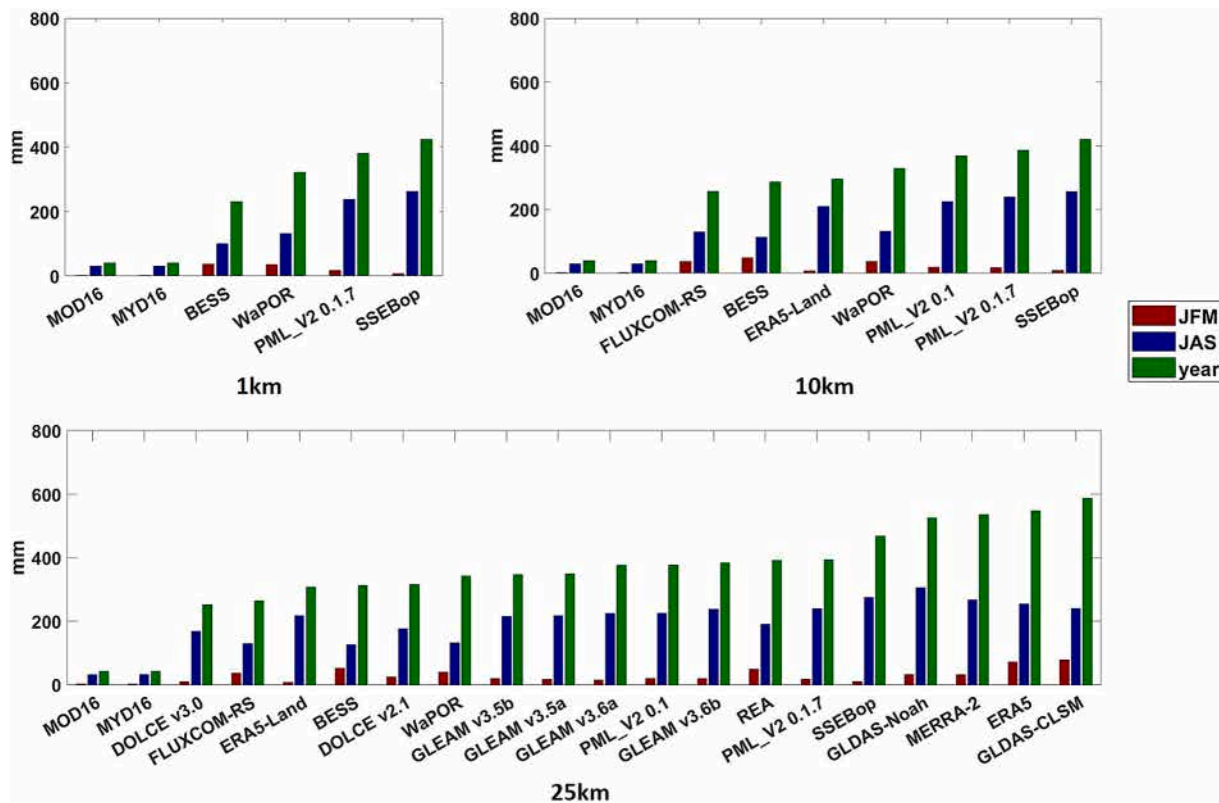
Fig. 10. Median of each product's spatial distribution on mean (2009–2015) annual and seasonal ET over dry (January to March) and wet (July to September) seasons over South-Western Niger at different spatial aggregation levels: 1 km (a), 10 km (b), 25 km (c).

products, with a quite consistent decorrelation throughout the seasons (R≈0.6). This decorrelation is also exacerbated at higher resolution with (R≈0.2). It may partly be due to the artefacts spotted around masked areas, but also and mainly by the low spatial variability displayed in Fig. 7. Beside these products, other products show good agreement on the spatial distribution at 25 km aggregation scale (R≈0.8–0.9) as well as at higher resolution, with R≈0.6–0.7 even at kilometric scale, despite the expected degradation of the correlation with the increase in resolution.

6. Discussion

The biggest challenge in evaluating gridded ET products is the scarcity of eddy-covariance measurements, which give very limited insight about the spatial patterns of ET. It is particularly true in Sahelian region, where the ET measurement network is very scarce. It raises the question of the representativity of such measurements at larger scale. In our study, the Faidherbia-flux and Wankama flux stations monitor ecosystems widely present in their respective study areas, thus providing good confidence on the generalizability of the conclusions on similar ecosystems at larger scale. It is shown by the good agreement between local scale scores and area scale cross-comparison of the products. However, conclusions could be very different on the wetland ecosystems, as in the Saloum delta or on the Niger river banks, that have a very different hydrometeorological behaviour. Another challenge to tackle is the mismatch between flux tower footprint and product's spatial grid (Miralles et al., 2011; Majozi et al., 2017; Allies et al., 2020). Indeed, the coarser the resolution, the higher the heterogeneity within the considered pixel and the mismatch between tower and satellite pixel footprints (McCabe and Wood, 2006). The openET initiative (Melton et al., 2022) aims at filling this gap by proposing methods, such as the DisALEXI algorithm (Anderson et al., 2011), to derive field scale ET from satellite data. But this initiative is up-to-now limited to the CONUS and needs to

be adapted to other regions. The comparison with flux tower measurements is also prone to measurements uncertainties, linked to the sensors' precision, the discrepancies between the different energy fluxes sensors (i.e. radiation, turbulent fluxes, ground heat flux) and the turbulence determination uncertainties, which often leads to an imbalance in the energy budget closure. The good energy budget closure of both flux tower's fluxes should limit the risk of having such uncertainties, although a good energy closure does not necessarily mean that ET is good in particular.

To this end, many studies have assessed the products capacities by comparing them to the monthly or yearly ET derived from water balance calculations on river catchments (Andam-Akorful et al., 2014; Bai and Liu, 2018; Chao et al., 2021). While it can be a relevant indicator, this type of comparison has many limitations. Firstly, ET is assumed to be the residual of the water balance, namely precipitation over the catchment minus discharge at its outflow, with the assumption that storage in the system is neglectable at the time scale considered. Hence, it depends heavily on the quality of discharge measurements. In addition, this assumption is particularly untrue over small aggregation time periods (under the month) or in catchments with groundwater fluctuations within the time period (Imbach et al., 2010). Chao et al. (2021) tackled this issue by using the GRACE satellite data to derive the groundwater fluctuations. Finally, such comparisons are catchment dependent and do not allow for comparisons outside these catchments, even though they may not sample every remarkable ecosystem. This emphasizes the necessity to analyse the spatial patterns of ET, although the wide variety of spatial and temporal resolution between products render it difficult. While good performing products should have a great temporal representation of the ET cycle while providing a realistic spatial distribution, their spatiotemporal characteristics can make them unfit for specific applications.

A multi-scale analysis is thus needed to evaluate the strengths and weaknesses of each product at different aggregation level and determine
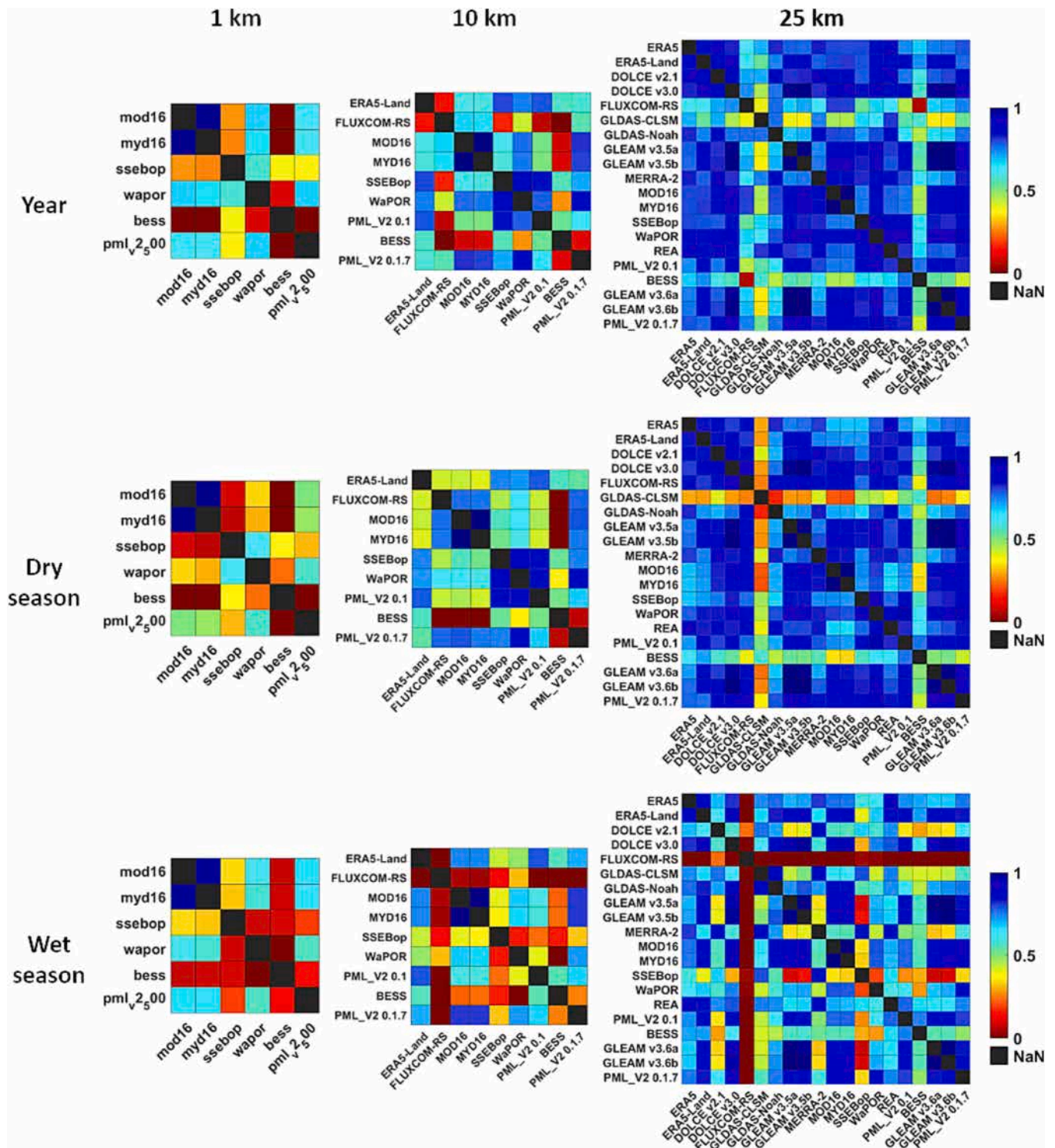
Fig. 11. Pearson correlation coefficient between each product spatial distribution on mean (2009–2015) annual (first row) and seasonal (second and third rows) ET over dry (January to March) and wet (July to September) seasons over Central Senegal at different spatial aggregation levels (1 km, 10 km, 25 km).

each product's most suitable field of application. For example, despite their low spatial and temporal resolution (0.25°, monthly), the DOLCE products, especially DOLCE v2.1, show good performances at local scale and good agreement with other good-performing products at mesoscale. It makes them particularly well fitted to long term trend analysis over large areas or to hydrological regime studies over very large catchments, such as in Hobeichi et al. (2021). The products with the highest temporal resolution, such as ERA5s, MERRA-2 and GLDAS are all dedicated to

large scale studies, making the link between Global Circulation Models and LSMs or hydrological models, explaining their low spatial resolution (≥0.25°). In this category, GLDAS-Noah seems to be one of the best performing products over croplands and savannah, probably due to the greater precision of their land surface scheme, but miss important effects on ET over the deltaic area in Central Senegal with wetland ecosystems. MERRA-2, despite having better scores at local scale, is hindered by its low spatial resolution (>0.5°), mixing too many ecosystems and even

open water (delta or coastal areas). Thus, its spatial analysis displays high over-estimations during the dry season. ERA5 product show similar behaviour than MERRA-2. Therefore, ERA5-Land seems to be the best compromise in this category, providing the best spatial resolution (0.1°), satisfactory performances at local scale and a realistic representation of spatial ET patterns. GLEAM products seem to be the best performing, even when looking at the local scale, despite their 0.25° resolution, confirming them as reference products in tropical semi-arid areas (Khan et al., 2020; Salazar-Martinez et al., 2022). However, as shown in the spatial analysis, the GLEAM products have a hard time describing the spatial patterns, even if the 0.25° pixels seem to be realistically influenced by their inner spatial heterogeneity. GLEAM products can thus be used in large scale hydrological studies as well as climate trends study, due to their great time span. But they can also be used for agricultural management purposes, allowing long term diagnostic studies with good temporal precision, provided the ecosystem is sufficiently homogeneous at the 0.25°-pixel scale (Allies et al., 2022). Higher resolution remote sensing products, such as BESS, MOD16/MYD16, PML_V2, SSEBop and WaPOR all displays lower performances. As these products provide data to a near kilometric resolution with weekly to decadal temporal resolution, their main field of application is the agricultural and water management at smaller scale (small catchments or agricultural perimeters). However, most of them do not seem adapted to Sahelian climate and ecosystems. That is particularly true for BESS, SSEBop and MOD16/MYD16 which show large biases and/or low spatial correlations with other products. These behaviours have been observed in other studies on different semi-arid ecosystems (Majozi et al., 2017; Bennour et al., 2022). WaPOR seems to be the best compromise within these high-resolution products in Central Senegal, showing middling performances at local scale but a realistic spatial distribution. For agricultural studies, which is the main scope of WaPOR, good local scale performances in agrosystems should however prevail over good spatial distribution. However, its performances drop in South-Western Niger. It should be noted that WaPOR beneficiates of hyper-resolute versions (30 m and 100 m) on parts of the Senegal, meaning the algorithm has been thoroughly calibrated in ecosystems very similar to the Niakhar station. It could explain the discrepancy on WaPOR ET performances on both sites/areas. Recent literature (Bennour et al., 2022) also suggests that WaPOR performances are quite lower on other areas, especially dryer ones.

Apart from spatiotemporal resolution differences, products performance discrepancies can be due to: the algorithms' principles, parameterization or forced/assimilated data. As shown in Section 5.2, products using precipitation fields might display spatiotemporal differences depending on this forcing. It seems to be the case for GLDAS products, which do not follow the precipitation spatial patterns of CHIRPS (Fig. 8). Several studies have shown that GLDAS precipitation forcing is not performing as well as CHIRPS when describing the spatio-temporal distribution of the precipitation over different region of the world, including African semi-arid countries (Wang et al., 2020, Degefu et al., 2022). Similar uncertainties can occur with other gridded data, e.g. vegetation indices, soil properties or other meteorological forcing. For example, PML_V2 products seem to have very different responses to parameterization between ecosystems, meaning they are very sensitive to input land cover maps. It is probably due to its algorithm functioning with separate plant functional types, derived from MCD12 land cover product (Friedl & Sulla-Menashe, 2022), with parameters calibrated over FLUXNET measurements with corresponding types. Concerning, MOD16/MYD16 and BESS products, land cover parameterization could also be a problem. Indeed, they also use MCD12 land cover product, or its past versions, which could be the source of their low spatial variations. The fact that, contrarily to BESS, MOD16/MYD16 algorithm does not use thermal information as a proxy of the water stress may explain its trend to deeply underestimate ET in our study areas, characterized by low vegetation indices, even in wet season. PML_V2 avoid this problem by including an information about anterior precipitations in its forcing.

The surface incoming radiation, used as an input by almost all products, is also recognized to be an important source of uncertainty in most ET model (Mira et al., 2016). The case of SSEBop is a great example of parameterization issues. Indeed, the SSEBop algorithm has been broadly tested and validated over a variety of ecosystems and input data (Chen et al., 2016; Dias Lopes et al., 2019; Zhuang et al., 2021; Senay et al., 2022). However, it relies on determining the ratio of surface temperature between actual and potential ET conditions. An overestimation of the temperature at potential ET conditions should induce greater ET over the entire area, especially during wet period. An underestimation of this temperature would conversely lead to ET underestimation in dry conditions. This is the behaviour observed on SSEBop in our study. Finally, some algorithms are more adapted to specific climatic conditions than others. Our results suggest that products that explicitly consider soil moisture evolution, like GLEAM, ERA-5 Land or GLDAS-Noah, tend to have better performances in the Sahelian region. This is not surprising as in semi-arid areas, ET is mainly water limited. The end of the crop season illustrates this point. Products that consider soil moisture tends to have longer ET cycle, that better fit local observations than other products. Indeed, rain usually stops two to three weeks before the ET cycle does in Sahel. Hence, this period's ET only consists in transpiration. Including soil moisture in the parameterization may then be an asset to better capture phases with transpiration only. Hence, accurately evaluating the soil moisture availability is crucial to ET estimation. It explains why products like MOD16/MYD16, which only uses vapor pressure deficit and relative air humidity to derive water stress, do not work well in semi-arid areas (Velpuri et al., 2013; Hu et al., 2015). Another problem for remote-sensing based algorithm is that visible and thermal Earth observation, on which these algorithms rely, is deeply affected by satellite revisit frequency and cloud coverage. It emphasizes even more the need for soil-moisture accounting to derive accurate continuous ET time series in periods with low satellite data availability.

7. Conclusion

The comparison of several ET products conducted in this study allowed to assess the qualities and drawbacks of each product to handle various scientific questions and applications in Sahelian context. This comparison was performed with a multi-scale analysis rarely seen in ET comparison studies but that is needed to tackle the spatio-temporal characteristics discrepancies between products. First, the temporal behaviour of the products was assessed through a local comparison to eddy-covariance measurements on ecosystems representative of Sahelian croplands in Central Senegal and South-Western Niger. Some products, like GLDAS-Noah, MERRA-2, the GLEAM products or ERA5-Land, stood out as good candidates to become reference products over these areas. The spatial analysis gave more credit to the two latter, having a more realistic representation of the spatial patterns of ET. Their long timespans are a strong asset for long term diagnostic analysis, be it for climatic studies or large-scale hydrology. However, their low spatial resolutions, respectively 0.25° and 0.1°, as well as their timing of production limits their usage for fine scale applications, such as agricultural monitoring and water management or small basin hydrology. On the other hand, more spatially resolute products (≤5km), dedicated to such applications, did not display good performances at local scale. In this category, all of the six products concerned (MOD16, MYD16, WaPOR, BESS, PML_V2 0.1.7 and SSEBop) have visible flaws, may it be on the temporal or spatial representativity. PML_V2 0.1.7 however seems to be the best compromise between local scale performances and spatial and temporal representativity. Overall, the comparison showed quantitative discrepancies between the products on par with the recent literature on semi-arid areas. This comparison should however be extended to larger scale in order to derive generalized conclusions to the entire climatic region and bring consensus about the reference products at such scale. Similar work is in progress over other West-African sites, sampling the

latitudinal and longitudinal climatic gradients. Nevertheless, the study highlights the need for products adapted to the Sahelian eco-climatic region, with both high spatiotemporal resolution and good representation of spatiotemporal ET patterns. It would be particularly relevant for agricultural and water management in a region where subsistence farming with sub-kilometric plots is predominant. Hydrological applications in the numerous small endoreic catchments would also be facilitated. A first promising approach to produce such product revolves around data fusion methods. The performances of the DOLCE products seem in line with this. Allies et al. (2022) already showed that combining large scale information from GLEAM with finer scale estimates from other algorithm drastically improves both the local scale performances and ET spatial distribution accuracy. Similar concepts could be used to combine the good temporal ET representation of GLEAM or GLDAS-Noah with the spatial information of more resolute products like WaPOR or SSEBop. A daily fusion product with kilometric resolution could thus be envisaged. By the way, recent and near future satellite missions, like TRISHNA (CNES/ISRO, Lagouarde et al., 2018), LSTM (ESA, Koetz et al., 2018) or SBG (NASA, Thompson et al., 2022), will provide even higher resolution data with spatial resolution of nearly 50 m and revisit frequency of two to three days each. Their combination should allow for the generation of well constrained ET products with remote-sensing based algorithms, such as contextual methods (Roerink et al., 2000; Carlson, 2007; Gallego-Elvira et al., 2013; Allies et al 2020) or single pixel methods (Bastiaanssen, 1995; Senay et al., 2013; Boulet el al., 2015) with less uncertainty due to interpolation/extrapolation between clear sky acquisitions.

CRediT authorship contribution statement

Jordi Etchanchu: Writing – original draft, Visualization, Validation, Software, Methodology, Formal analysis, Conceptualization. **Jérôme Demarty:** Writing – review & editing, Supervision, Project administration, Formal analysis, Conceptualization. **Alain Dezetter:** Writing – review & editing, Project administration, Methodology, Funding acquisition. **Nesrine Farhani:** Writing – review & editing, Software. **Pape Biteye Thiam:** Software, Methodology, Formal analysis. **Aubin Allies:** Writing – review & editing, Conceptualization. **Ansoumana Bodian:** Writing – review & editing. **Gilles Boulet:** Writing – review & editing, Project administration, Conceptualization. **Nanée Chahinian:** Writing – review & editing, Supervision. **Lamine Diop:** Writing – review & editing. **Ibrahim Mainassara:** Writing – review & editing, Data curation. **Pape Malick Ndiaye:** Writing – review & editing, Formal analysis. **Chloé Ollivier:** Writing – review & editing, Data curation. **Albert Olioso:** Writing – review & editing, Project administration, Conceptualization. **Olivier Roupsard:** Writing – review & editing, Resources, Data curation.

Declaration of competing interest

The authors declare that they have no known competing financial interests or personal relationships that could have appeared to influence the work reported in this paper.

Acknowledgment

Appendix A:. Description of the gridded ET products

A.1. Breathing Earth system Simulation (BESS)

BESS (Ryu et al., 2011; Jiang et Ryu., 2016) is an ET and Gross Primary Production (GPP) product generated globally on a 1 km resolution grid matching the MODIS products 1 km grid. Its temporal resolution is 8 days. Its estimations rely on a radiative transfer model within the atmosphere and the canopy, coupled with photosynthesis and canopy conductance models. ET is derived with the quadratic form of the Penman-Monteith equation (Monteith, 1965; Paw U & Gao, 1988) for latent heat flux. Most of the atmospheric and surface characteristics are derived from MODIS products. Missing atmospheric variables are derived from NCEP/NCAR meteorological reanalysis (Kalnay et al., 1996) while global classification maps are used to define the biomes and photosynthesis types (C3, C4).

A.2. Global Land Evaporation: The Amsterdam methodology (GLEAM)

GLEAM is a method to derive global ET at a daily timescale and 0.25° resolution from a wide range of satellite observations (Miralles et al., 2011). The GLEAM algorithm estimates the potential ET with a modified Priestley-Taylor formulation (Priestley and Taylor, 1972). The actual ET is then derived through the use of three main modules. In the first one, canopy interception is computed using a Gash model (Miralles et al., 2010). The second one consists of a soil module describing rain water infiltration where microwave-derived soil moisture data are assimilated in the top soil layer through a Kalman filter. The last module computes a stress factor function of root zone soil moisture derived from the soil module and remotely sensed vegetation optical depth. Actual evapotranspiration is finally computed as the sum of evaporation from the water intercepted by the canopy and potential ET multiplied by the stress factor. In this study, the 3.5a, 3.5b, 3.6a and 3.6b versions are used (Martens et al., 2017). In the GLEAM 3.5a and 3.6a products, inputs are taken from reanalysis (incoming radiation and air temperature), remote sensing data (soil moisture, vegetation optical depth and surface vegetation cover), field survey (soil properties) and merged remote sensing and ground-based precipitations. In the 3.5b and 3.6b versions, all inputs, except soil properties are derived from remote sensing data. The difference between the 3.5 and 3.6 products is the use of more up-to-date precipitation, soil moisture, vegetation optical depth, radiation and temperature data.

A.3. MODIS Global evapotranspiration products (MOD16/MYD16)

The MODIS Global Evapotranspiration product (MOD16, Mu et al., 2007, 2011) is provided by the Earth Observing System of the National Aeronautics and Space Administration (NASA/EOS). The MOD16 algorithm is based on a modified Penman-Monteith (Monteith, 1965) approach to

derive potential ET. A biome specific model is then used to compute surface resistance to evapotranspiration on plants and bare soil, and consequently actual ET, without calculating the entire surface water and/or energy budget. The biomes and vegetation variables are derived from MODIS products on land cover and vegetation indices (LAI/FPAR) while atmospheric conditions are derived from the GMAO reanalysis data (Zhao et al., 2005). In this study the MOD16A2v061 and MYD16A2v061 versions are used, which provide ET at 8-day with a spatial resolution of 500 m, respectively using the TERRA and AQUA satellites.

A.4. Penman-Monteith Leuning version 2 (PML_V2)

PML combined the Penman-Monteith equation and the surface conductance model of (Leuning et al., 2008) to derive evapotranspiration as a sum of canopy transpiration, soil evaporation and evaporation of precipitation intercepted by the vegetation. In this study we used the PML_V2 (Zhang Y. et al., 2010, 2016, 2019) product that uses a water-carbon coupled canopy conductance to derive canopy transpiration and gross primary production. It uses GLDAS_v2.1 meteorological forcing (Beaudoing and Rodell, 2020) and MODIS collection 6 products (LAI, albedo, surface emissivity and land cover types) as forcing data. PML_V2 ET is provided at 8-day with both 0.05° (PML_V2 0.1) and 500 m (PML_V2 0.1.7) resolution.

A.5. Simplified surface energy balance for operational applications (SSEBop)

The SSEBop (Senay et al., 2013) ET product is based on the one-source surface energy balance model. In this model actual evapotranspiration per-pixel is derived from the evaporative fraction. The latter is computed by a linear relationship on the difference between land surface temperature (LST) of the pixel and the coldest/wettest surface temperature limit in the satellite image. The evaporative fraction is multiplied by the reference evapo-transpiration for alfalfa to obtained actual evapotranspiration. SSEBop global ET product used decadal 1-km MODIS LST and surface/vegetation products (NDVI, albedo, emissivity) while air temperature is derived from WorldClim (Fick and Hijmans, 2017). ET0 was provided by the USGS Famine Early Warning Systems Network (FEWS NET) Data Portal (https://earlywarning.usgs.gov/fews/product/81) at 100 km spatial resolution and downscaled at 10 km spatial resolution using spatial patterns and statistics derived from potential ET provided by the InternationalWater Management Institute (IWMI) (Senay et al., 2007). SSEBop ET is provided at 1 km spatial resolution and 10-days timestep.

A.6. Water productivity through open access of remotely sensed derived data (WaPOR)

WaPOR ET (FAO, 2020) is based on a modified version of the ETLook model developed by (Bastiaanssen et al., 2012). ETLook uses a Penman-Monteith (Monteith, 1965) approach to determine actual ET separately for bare soil evaporation and canopy transpiration by solving the energy budget in each case, with a classical surface resistance scheme (Jarvis, 1976). The surface and root-zone soil moisture are also considered by a stress factor in the canopy resistance computed on the base of NDVI/LST relationship, also known as triangle method (Carlson, 2007), with a method described by Yang Y. et al. (2015). WaPOR uses MODIS daily surface reflectance, LST and emissivity, Climate Hazards Group Infrared Precipitation with Station Data (CHIRPS) precipitation data and Digital Elvetation Model from the Shuttle Radar Topography Mission (SRTM) as inputs. WaPOR ET for continental Africa is provided at 250 m resolution and decadal timestep. Some subregions are provided at 100 m but as this does not include all of our study area, we did not use it. A research version at 30 m resolution is also available on very specific areas.

A.7. ERA5 and ERA5-Land

ERA5 (Hersbach et al., 2020, 2023) is a global climate and weather reanalysis proposed by the European Center for Medium-range Weather Forecasts (ECMWF). It uses a data assimilation system to constrain a global circulation and atmospheric model with various observational data. The H-TESSEL (Balsamo et al., 2009) Land Surface Model (LSM) is used to determine the surface boundary condition fluxes, including ET. The variables are provided hourly at a 0.25° spatial resolution. ERA5-Land (Muñoz-Sabater et al., 2019, 2021) is derived from ERA5 atmospheric variables by rerunning the land surface model at higher resolution (0.1°).

A.8. Global Land data Assimilation system (GLDAS)

The Global Land Data Assimilation System (GLDAS, Rodell et al., 2004) provides gridded land surface state variables and fluxes by assimilating satellite and ground based observations into different LSMs. In the 2.1 version (Beaudoing and Rodell, 2020), used in this study, four LSMs are driven in GLDAS: Noah (Ek et al., 2003), Catchment Land Surface Model (CLSM, Ducharne et al., 2000; Koster et al, 2000), Community Land Model (CLM, Dai et al., 2003) and Variable Infiltration Capacity (VIC, Liang et al, 1994). These models are forced with the National Oceanic and Atmospheric Administration (NOAA) atmospheric reanalysis. Only the two first LSMs (Noah and CLSM) are used in the study as they run at 0.25° resolution instead of 1° for the two last (CLM and VIC). The temporal resolution of GLDAS-Noah is 3 h while GLDAS-CLSM provides daily estimations.

A.9. Modern-Era Retrospective analysis for research and applications v2 (MERRA-2)

MERRA-2 (GMAO, 2015; Gelaro et al., 2017) is a reanalysis dataset produced by the NASA Global Modeling and Assimilation Office (GMAO). It uses a data assimilation system to incorporate various ground-based and remotely sensed observation datasets within the Goddard Earth Observing System version 5 (GEOS-5) general circulation model (Rienecker et al., 2008; Molod et al., 2015). The land surface component is computed with the CLSM (Ducharne et al., 2000; Koster et al, 2000) model. The variables, including ET, are distributed hourly at a 0.5° by 0.625° resolution.

A.10. FLUXCOM-RS

The FLUXCOM initiative (Jung et al., 2019, 2020) provides gridded surface flux products globally. The concept is to upscale FLUXNET flux tower measurements (Pastorello et al., 2020) with machine learning methods (Tramontana et al., 2016). These upscaling methods use satellite remote sensing and meteorological data as inputs. They were trained using field measurements from 224 flux tower beforehand corrected from energy balance non-closure using three correction variants. Two versions of products are delivered by considering different setups of input drivers. The FLUXCOM-RS

product fluxes are estimated using exclusively MODIS remote sensing data in the upscaling methods. It allows for a precise spatial resolution (0.0833°) but with an 8-day temporal resolution and a reduced timespan (2000–2015). The FLUXCOM-RS + METEO uses the gridded meteorological data combined with mean seasonal cycles derived from MODIS remote sensing data. This setup allows for a better temporal resolution (day) and a greater timespan (1980–2013) but with a coarser spatial resolution (0.5°). As the spatial resolution is lower and the timespan only goes to 2013 for this product, only the FLUXCOM-RS is used in this study.

A.11. Derive Optimal linear combination evapotranspiration (DOLCE)

DOLCE (Hobeichi et al., 2018) is a monthly 0.25° gridded ET product generated by computing a linear combination of several existing ET products. The method consists in an ensemble weighting and rescaling technique that allows the linear combination of the ensemble members. The aim is to minimize the mean square error when compared to a dataset composed of ground measurements acquired on 260 flux tower sites from different global and regional flux tower networks. These measurements have been previously corrected from energy imbalance using the Bowen Ratio method (Twine et al., 2000). Two versions of the DOLCE products are used in this study. DOLCE v2.1 (Hobeichi, 2020) combines the following datasets: BACI (Bodesheim et al., 2018), FLUXCOM-RS and RS + METEO (Jung et al., 2019, 2020), ERA5-Land (Muñoz-Sabater et al., 2019, 2021), GLEAM versions 3.3a and 3.3b (Miralles et al., 2011; Martens et al., 2017) PML-CSIRO (Zhang K. et al., 2016), PSLH, MOD16A2 (Mu et al., 2011), SEBS (Su, 2002) and SRB-GEWEX (Cox et al., 2017). On the other hand, DOLCE v3.0 (Hobeichi, 2021) only combines 4 datasets: ERA5-Land, FLUXCOM-RS and RS + METEO and GLEAM v3.5a and 3.5b, in order to ensure temporal consistency over the entire proposed period (1981–2018).

A.12. Reliability ensemble averaging (REA)

The REA ET product (Lu et al., 2021) is based on the weighed combination of ECMWF ERA5 (Hersbach et al., 2020), GLDAS2-Noah (Beaudoing and Rodell, 2020; Rodell et al., 2004) and MERRA2 (Gelaro et al., 2017) estimations using Reliability Ensemble Averaging (REA) method considering both model performance and model convergence as reliability criteria. Model convergence is based on the distance between the ET product ensemble member and the ensemble average. Model performance is the bias between simulated ET and a reference. Instead of flux tower measurements, REA used GLEAM v3.0 (Martens et al., 2017) ET estimates as reference allowing a merging at pixel scale. REA ET are provided at 0.25° spatial resolution and daily timescale.
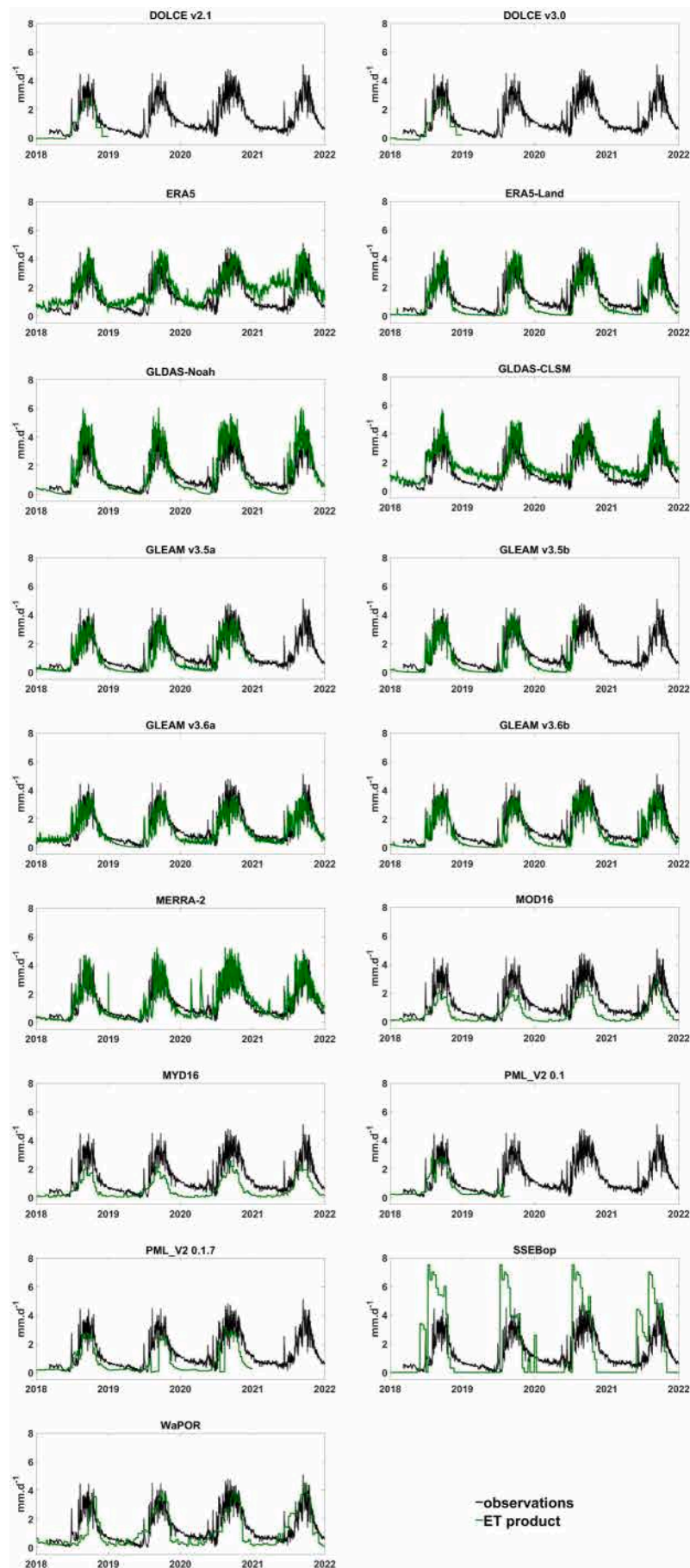
Fig. B1. Temporal series of the products at the Niakhar flux station over the 20182021 period

Data availability

Datasets are available on their producers sites, indicated by the links provided in the article

References

Adeyeri, O.E., Ishola, K.A., 2021. Variability and Trends of Actual Evapotranspiration over West Africa: The Role of Environmental Drivers. Agric. For. Meteorol. 308–309, 108574. https://doi.org/10.1016/j.agrformet.2021.108574.

Alemohammad, S.H., Fang, B., Konings, A.G., Aires, F., Green, J.K., Kolassa, J., Miralles, D., Prigent, C., Gentine, P., 2017. Water, Energy, and Carbon with Artificial Neural Networks (WECANN): A statistically-based estimate of global surface turbulent fluxes and gross primary productivity using solar-induced fluorescence. Biogeosciences 14, 4101–4124. https://doi.org/10.5194/bg-14-4101-2017.

Alfieri, J.G., Anderson, M.C., Kustas, W.P., Cammalleri, C., 2017. Effect of the revisit interval and temporal upscaling methods on the accuracy of remotely sensed evapotranspiration estimates. Hydrol. Earth Syst. Sci. 21, 83–98. https://doi.org/10.5194/hess-21-83-2017.

Allies, A., Demarty, J., Olioso, A., Bouzou Moussa, I., Issoufou, H.-B.-A., Velluet, C., Bahir, M., Maïnassara, I., Oï, M., Chazarin, J.-P., Cappelaere, B., 2020. Evapotranspiration Estimation in the Sahel Using a New Ensemble-Contextual Method. Remote Sens. (Basel) 12, 380. https://doi.org/10.3390/w2020170.

Allies, A., Olioso, A., Cappelaere, B., Boulet, G., Etchanchu, J., Barral, H., Bouzou Moussa, I., Chazarin, J.-P., Delogu, E., Issoufou, H.-B.-A., Mainassara, I., Oï, M., Demarty, J., 2022. A remote sensing data fusion method for continuous daily evapotranspiration mapping at kilometric scale in Sahelian areas. J. Hydrol. 607, 127504. https://doi.org/10.1016/j.jhydrol.2022.127504.

Amogu, O., Descroix, L., Yéro, K.S., Le Breton, E., Mamadou, I., Ali, A., Vischel, T., Bader, J.-C., Moussa, I.B., Gautier, E., Boubkraoui, S., Belleudy, P., 2010. Increasing River Flows in the Sahel? Water 2, 170–199. https://doi.org/10.3390/w2020170.

Andam-Akorful, S.A., Ferreira, V.G., Awange, J.L., Forootan, E., He, X.F., 2015. Multi-model and multi-sensor estimations of evapotranspiration over the Volta Basin, West Africa. Int. J. Climatol. 35, 3132–3145. https://doi.org/10.1002/joc.4198.

Anderson, M.C., Kustas, W.P., Norman, J.M., Hain, C.R., Mecikalski, J.R., Schultz, L., González-Dugo, M.P., Cammalleri, C., d'Urso, G., Pimstein, A., Gao, F., 2011. Mapping daily evapotranspiration at field to continental scales using geostationary and polar orbiting satellite imagery. Hydrol. Earth Syst. Sci. 15, 223–239. https://doi.org/10.5194/hess-15-223-2011.

Bado, B.V., Whitbread, A., Sanoussi Manzo, M.L., 2021. Improving agricultural productivity using agroforestry systems: Performance of millet, cowpea, and ziziphus-based cropping systems in West Africa Sahel. Agr Ecosyst Environ 305, 107175. https://doi.org/10.1016/j.agee.2020.107175.

Bai, P., Liu, X., 2018. Intercomparison and evaluation of three global high-resolution evapotranspiration products across China. J. Hydrol. 566, 743–755. https://doi.org/10.1016/j.jhydrol.2018.09.065.

Balsamo, G., Beljaars, A., Scipal, K., Viterbo, P., van den Hurk, B., Hirschi, M., Betts, A.K., 2009. A Revised Hydrology for the ECMWF Model: Verification from Field Site to Terrestrial Water Storage and Impact in the Integrated Forecast System. J. Hydrometeorol. 10, 623–643. https://doi.org/10.1175/2008JHM1068.1.

Bastiaanssen, W.G.M., 1995. Regionalization of surface flux densities and moisture indicators in composite terrain : a remote sensing approach under clear skies in Mediterranean climates (phd). Wageningen, SC-DLO.

Bastiaanssen, W.G.M., Cheema, M.J.M., Immerzeel, W.W., Miltenburg, I.J., Pelgrum, H., 2012. Surface energy balance and actual evapotranspiration of the transboundary Indus Basin estimated from satellite measurements and the ETLook model. Water Resour. Res. 48. https://doi.org/10.1029/2011WR010482.

H.K. Beaudoing M. Rodell GLDAS Noah Land Surface Model L4 3 Hourly 0.25 x 0.25 Degree V2.1 2020 Greenbelt, Maryland, USA, Goddard.

Bennour, A., Jia, L., Menenti, M., Zheng, C., Zeng, Y., Asenso Barnieh, B., Jiang, M., 2022. Calibration and Validation of SWAT Model by Using Hydrological Remote Sensing Observables in the Lake Chad Basin. Remote Sens. (Basel) 14, 1511. https://doi.org/10.3390/rs14061511.

Bodesheim, P., Jung, M., Gans, F., Mahecha, M.D., Reichstein, M., 2018. Upscaled diurnal cycles of land–atmosphere fluxes: a new global half-hourly data product. Earth Syst. Sci. Data 10, 1327–1365. https://doi.org/10.5194/essd-10-1327-2018.

Bodian, A., Diop, L., Panthou, G., Dacosta, H., Deme, A., Dezetter, A., Ndiaye, P.M., Diouf, I., Vischel, T., 2020. Recent Trend in Hydroclimatic Conditions in the Senegal River Basin. Water 12, 436. https://doi.org/10.3390/w12020436.

Bombelli, A., Henry, M., Castaldi, S., Adu-Bredu, S., Arneth, A., de Grandcourt, A., Grieco, E., Kutsch, W.L., Lehsten, V., Rasile, A., Reichstein, M., Tansey, K., Weber, U., Valentini, R., 2009. An outlook on the Sub-Saharan Africa carbon balance. Biogeosciences 6, 2193–2205. https://doi.org/10.5194/bg-6-2193-2009.

Boulet, G., Mougenot, B., Lhomme, J.-P., Fanise, P., Lili-Chabaane, Z., Olioso, A., Bahir, M., Rivalland, V., Jarlan, L., Merlin, O., Coudert, B., Er-Raki, S., Lagouarde, J.-P., 2015. The SPARSE model for the prediction of water stress and evapotranspiration components from thermal infra-red data and its evaluation over

irrigated and rainfed wheat. Hydrol. Earth Syst. Sci. 19, 4653–4672. https://doi.org/10.5194/hess-19-4653-2015.

Cammalleri, C., Anderson, M.C., Gao, F., Hain, C.R., Kustas, W.P., 2013. A data fusion approach for mapping daily evapotranspiration at field scale. Water Resour. Res. 49, 4672–4686. https://doi.org/10.1002/wrcr.20349.

Cappelaere, B., Descroix, L., Lebel, T., Boulain, N., Ramier, D., Laurent, J.-P., Favreau, G., Boubkraoui, S., Boucher, M., Bouzou Moussa, I., Chaffard, V., Hiernaux, P., Issoufou, H.B.A., Le Breton, E., Mamadou, I., Nazoumou, Y., Oi, M., Ottlé, C., Quantin, G., 2009. The AMMA-CATCH experiment in the cultivated Sahelian area of south-west Niger – Investigating water cycle response to a fluctuating climate and changing environment. Journal of Hydrology, Surface Processes and Water Cycle in West Africa, Studied from the AMMA-CATCH Observing System 375, 34–51. https://doi.org/10.1016/j.jhydrol.2009.06.021.

Cawse-Nicholson, K., Anderson, M.C., Yang, Y., Yang, Y., Hook, S.J., Fisher, J.B., Halverson, G., Hulley, G.C., Hain, C., Baldocchi, D.D., Brunsell, N.A., Desai, A.R., Griffis, T.J., Novick, K.A., 2021. Evaluation of a CONUS-Wide ECOSTRESS DisALEXI Evapotranspiration Product. IEEE J. Sel. Top. Appl. Earth Obs. Remote Sens. 14, 10117–10133. https://doi.org/10.1109/JSTARS.2021.3111867.

Chagnaud, G., Panthou, G., Vischel, T., Lebel, T., 2022. A synthetic view of rainfall intensification in the West African Sahel. Environ. Res. Lett. 17, 044005. https://doi.org/10.1088/1748-9326/ac4a9c.

Chao, L., Zhang, K., Wang, J., Feng, J., Zhang, M., 2021. A Comprehensive Evaluation of Five Evapotranspiration Datasets Based on Ground and GRACE Satellite Observations: Implications for Improvement of Evapotranspiration Retrieval Algorithm. Remote Sens. (Basel) 13, 2414. https://doi.org/10.3390/rs13122414.

Chen, M., Senay, G.B., Singh, R.K., Verdin, J.P., 2016. Uncertainty analysis of the Operational Simplified Surface Energy Balance (SSEBop) model at multiple flux tower sites. J. Hydrol. 536, 384–399. https://doi.org/10.1016/j.jhydrol.2016.02.026.

Cox, S.J., Stackhouse, P.W., Gupta, S.K., Mikovitz, J.C., Zhang, T., 2017. NASA/GEWEX shortwave surface radiation budget: Integrated data product with reprocessed radiance, cloud, and meteorology inputs, and new surface albedo treatment. AIP Conference Proceedings 1810, 090001. https://doi.org/10.1063/1.4975541.

Dai, Y., Zeng, X., Dickinson, R.E., Baker, I., Bonan, G.B., Bosilovich, M.G., Denning, A.S., Dirmeyer, P.A., Houser, P.R., Niu, G., Oleson, K.W., Schlosser, C.A., Yang, Z.-L., 2003. The Common Land Model. Bull. Am. Meteorol. Soc. 84, 1013–1024. https://doi.org/10.1175/BAMS-84-8-1013.

Degefu, M.A., Bewket, W., Amha, Y., 2022. Evaluating performance of 20 global and quasi-global precipitation products in representing drought events in Ethiopia I: Visual and correlation analysis. Weather Clim. Extremes 35, 100416. https://doi.org/10.1016/j.wace.2022.100416.

Delogu, E., Olioso, A., Alliès, A., Demarty, J., Boulet, G., 2021. Evaluation of Multiple Methods for the Production of Continuous Evapotranspiration Estimates from TIR Remote Sensing. Remote Sens. (Basel) 13, 1086. https://doi.org/10.3390/rs13061086.

Dembélé, M., Zwart, S.J., 2016. Evaluation and comparison of satellite-based rainfall products in Burkina Faso, West Africa. Int. J. Remote Sens. 37, 3995–4014. https://doi.org/10.1080/01431161.2016.1207258.

Dias Lopes, J., Neiva Rodrigues, L., Acioli Imbuzeiro, H.M., Falco Pruski, F., 2019. Performance of SSEBop model for estimating wheat actual evapotranspiration in the Brazilian Savannah region. Int. J. Remote Sens. 40, 6930–6947. https://doi.org/10.1080/01431161.2019.1597304.

Diongue, D.M.L., Roupsard, O., Do, F.C., Stumpp, C., Orange, D., Sow, S., Jourdan, C., Faye, S., 2022. Evaluation of parameterisation approaches for estimating groundnut basin hydraulic parameters with HYDRUS-1D in the groundnut basin of Senegal. Hydrol. Sci. J. 67, 2327–2343. https://doi.org/10.1080/02626667.2022.2142474.

Diop, L., Bodian, A., Diallo, D., 2016. Spatiotemporal Trend Analysis of the Mean Annual Rainfall in Senegal. European Scientific Journal, ESJ 12, 231. https://doi.org/10.19044/esj.2016.v12n12p231.

Droppelmann, K.J., Snapp, S.S., Waddington, S.R., 2017. Sustainable intensification options for smallholder maize-based farming systems in sub-Saharan Africa. Food Sec. 9, 133–150. https://doi.org/10.1007/s12571-016-0636-0.

Ducharne, A., Koster, R.D., Suarez, M.J., Stieglitz, M., Kumar, P., 2000. A catchment-based approach to modeling land surface processes in a general circulation model: 2. Parameter estimation and model demonstration. J. Geophys. Res. Atmos. 105, 24823–24838. https://doi.org/10.1029/2000JD900328.

Ek, M.B., Mitchell, K.E., Lin, Y., Rogers, E., Grunmann, P., Koren, V., Gayno, G., Tarpley, J.D., 2003. Implementation of Noah land surface model advances in the National Centers for Environmental Prediction operational mesoscale Eta model. J. Geophys. Res. Atmos. 108. https://doi.org/10.1029/2002JD003296.

Ershadi, A., McCabe, M.F., Evans, J.P., Chaney, N.W., Wood, E.F., 2014. Multi-site evaluation of terrestrial evaporation models using FLUXNET data. Agric. For. Meteorol. 187, 46–61. https://doi.org/10.1016/j.agrformet.2013.11.008.

Fick, S.E., Hijmans, R.J., 2017. WorldClim 2: new 1-km spatial resolution climate surfaces for global land areas. Int. J. Climatol. 37, 4302–4315. https://doi.org/10.1002/joc.5086.

Friedl, M., D. Sulla-Menashe, 2022. MODIS/Terra+Aqua Land Cover Type Yearly L3 Global 500m SIN Grid V061, distributed by NASA EOSDIS Land Processes Distributed Active Archive Center, https://doi.org/10.5067/MODIS/MCD12Q1.061.

Funk, C., Peterson, P., Landsfeld, M., Pedreros, D., Verdin, J., Shukla, S., Husak, G., Rowland, J., Harrison, L., Hoell, A., Michaelsen, J., 2015. The climate hazards infrared precipitation with stations—a new environmental record for monitoring extremes. Sci. Data 2, 150066. https://doi.org/10.1038/sdata.2015.66.

Gallego-Elvira, B., Olioso, A., Mira, M., Castillo, S.R., Boulet, G., Marloie, O., Garrigues, S., Courault, D., Weiss, M., Chauvelon, P., Boutron, O., 2013. EVASPA (EVapotranspiration Assessment from SPAce) Tool: An overview. Procedia Environmental Sciences, Four Decades of Progress in Monitoring and Modeling of Processes in the Soil-Plant-Atmosphere System: Applications and Challenges 19, 303–310. https://doi.org/10.1016/j.proenv.2013.06.035.

García-Santos, V., Sánchez, J.M., Cuxart, J., 2022. Evapotranspiration Acquired with Remote Sensing Thermal-Based Algorithms: A State-of-the-Art Review. Remote Sens. (Basel) 14, 3440. https://doi.org/10.3390/rs14143440.

Gelaro, R., McCarty, W., Suárez, M.J., Todling, R., Molod, A., Takacs, L., Randles, C.A., Darmenov, A., Bosilovich, M.G., Reichle, R., Wargan, K., Coy, L., Cullather, R., Draper, C., Akella, S., Buchard, V., Conaty, A., da Silva, A.M., Gu, W., Kim, G.-K., Koster, R., Lucchesi, R., Merkova, D., Nielsen, J.E., Partyka, G., Pawson, S., Putman, W., Rienecker, M., Schubert, S.D., Sienkiewicz, M., Zhao, B., 2017. The Modern-Era Retrospective Analysis for Research and Applications, Version 2 (MERRA-2). J. Clim. 30, 5419–5454. https://doi.org/10.1175/JCLI-D-16-0758.1.

Guzinski, R., Nieto, H., Ramo Sánchez, R., Sánchez, J.M., Jomaa, I., Zitouna-Chebbi, R., Roupsard, O., López-Urrea, R., 2023. Improving field-scale crop actual evapotranspiration monitoring with Sentinel-3, Sentinel-2, and Landsat data fusion. Int. J. Appl. Earth Obs. Geoinf. 125, 103587. https://doi.org/10.1016/j.jag.2023.103587.

Hersbach, H., Bell, B., Berrisford, P., Hirahara, S., Horányi, A., Muñoz-Sabater, J., Nicolas, J., Peubey, C., Radu, R., Schepers, D., Simmons, A., Soci, C., Abdalla, S., Abellan, X., Balsamo, G., Bechtold, P., Biavati, G., Bidlot, J., Bonavita, M., De Chiara, G., Dahlgren, P., Dee, D., Diamantakis, M., Dragani, R., Flemming, J., Forbes, R., Fuentes, M., Geer, A., Haimberger, L., Healy, S., Hogan, R.J., Hólm, E., Janisková, M., Keeley, S., Laloyaux, P., Lopez, P., Lupu, C., Radnoti, G., de Rosnay, P., Rozum, I., Vamborg, F., Villaume, S., Thépaut, J.-N., 2020. The ERA5 global reanalysis. Q. J. R. Meteorolog. Soc. 146, 1999–2049. https://doi.org/10.1002/qj.3803.

Hersbach, H., Bell, B., Berrisford, P., Biavati, G., Horányi, A., Muñoz Sabater, J., Nicolas, J., Peubey, C., Radu, R., Rozum, I., Schepers, D., Simmons, A., Soci, C., Dee, D., Thépaut, J-N., 2023. ERA5 hourly data on single levels from 1940 to present. Copernicus Climate Change Service (C3S) Climate Data Store (CDS), 10.24381/cds.adbb2d47.

Hobeichi, S., Abramowitz, G., Evans, J., Ukkola, A., 2018. Derived Optimal Linear Combination Evapotranspiration (DOLCE): a global gridded synthesis ET estimate. Hydrol. Earth Syst. Sci. 22, 1317–1336. https://doi.org/10.5194/hess-22-1317-2018.

Hobeichi, S., Abramowitz, G., Evans, J.P., 2021. Robust historical evapotranspiration trends across climate regimes. Hydrol. Earth Syst. Sci. 25, 3855–3874. https://doi.org/10.5194/hess-25-3855-2021.

S. Hobeichi Derived Optimal Linear Combination Evapotranspiration - DOLCE 2020 https://doi.org/10.25914/5f1664837ef06.

S. Hobeichi Derived Optimal Linear Combination Evapotranspiration - DOLCE 2021 https://doi.org/10.25914/606e9120c5ebe.

Hu, G., Jia, L., Menenti, M., 2015. Comparison of MOD16 and LSA-SAF MSG evapotranspiration products over Europe for 2011. Remote Sens. Environ. 156, 510–526. https://doi.org/10.1016/j.rse.2014.10.017.

Imbach, P., Molina, L., Locatelli, B., Roupsard, O., Ciais, P., Corrales, L., Mahé, G., 2010. Climatology-based regional modelling of potential vegetation and average annual long-term runoff for Mesoamerica. Hydrol. Earth Syst. Sci. 14, 1801–1817. https://doi.org/10.5194/hess-14-1801-2010.

Inglada, J., Arias, M., Tardy, B., Hagolle, O., Valero, S., Morin, D., Dedieu, G., Sepulcre, G., Bontemps, S., Defourny, P., Koetz, B., 2015. Assessment of an Operational System for Crop Type Map Production Using High Temporal and Spatial Resolution Satellite Optical Imagery. Remote Sens. (Basel) 7, 12356–12379. https://doi.org/10.3390/rs70912356.

Jayne, T.S., Snapp, S., Place, F., Sitko, N., 2019. Sustainable agricultural intensification in an era of rural transformation in Africa. Glob. Food Sec. 20, 105–113. https://doi.org/10.1016/j.gfs.2019.01.008.

Jiang, C., Ryu, Y., 2016. Multi-scale evaluation of global gross primary productivity and evapotranspiration products derived from Breathing Earth System Simulator (BESS). Remote Sens. Environ. 186, 528–547. https://doi.org/10.1016/j.rse.2016.08.030.

Jiménez, C., Prigent, C., Mueller, B., Seneviratne, S.I., McCabe, M.F., Wood, E.F., Rossow, W.B., Balsamo, G., Betts, A.K., Dirmeyer, P.A., Fisher, J.B., Jung, M., Kanamitsu, M., Reichle, R.H., Reichstein, M., Rodell, M., Sheffield, J., Tu, K., Wang, K., 2011. Global intercomparison of 12 land surface heat flux estimates. J. Geophys. Res. Atmos. 116. https://doi.org/10.1029/2010JD014545.

Jung, M., Reichstein, M., Bondeau, A., 2009. Towards global empirical upscaling of FLUXNET eddy covariance observations: validation of a model tree ensemble approach using a biosphere model. Biogeosciences 6, 2001–2013. https://doi.org/10.5194/bg-6-2001-2009.

Jung, M., Koirala, S., Weber, U., Ichii, K., Gans, F., Camps-Valls, G., Papale, D., Schwalm, C., Tramontana, G., Reichstein, M., 2019. The FLUXCOM ensemble of global land-atmosphere energy fluxes. Sci. Data 6, 74. https://doi.org/10.1038/s41597-019-0076-8.

Jung, M., Schwalm, C., Migliavacca, M., Walther, S., Camps-Valls, G., Koirala, S., Anthoni, P., Besnard, S., Bodesheim, P., Carvalhais, N., Chevallier, F., Gans, F., Goll, D.S., Haverd, V., Köhler, P., Ichii, K., Jain, A.K., Liu, J., Lombardozzi, D., Nabel, J.E.M.S., Nelson, J.A., O'Sullivan, M., Pallandt, M., Papale, D., Peters, W., Pongratz, J., Rödenbeck, C., Sitch, S., Tramontana, G., Walker, A., Weber, U.,

Reichstein, M., 2020. Scaling carbon fluxes from eddy covariance sites to globe: synthesis and evaluation of the FLUXCOM approach. Biogeosciences 17, 1343–1365. https://doi.org/10.5194/bg-17-1343-2020.

Kalnay, E., Kanamitsu, M., Kistler, R., Collins, W., Deaven, D., Gandin, L., Iredell, M., Saha, S., White, G., Woollen, J., Zhu, Y., Chelliah, M., Ebisuzaki, W., Higgins, W., Janowiak, J., Mo, K.C., Ropelewski, C., Wang, J., Leetmaa, A., Reynolds, R., Jenne, R., Joseph, D., 1996. The NCEP/NCAR 40-Year Reanalysis Project. Bull. Am. Meteorol. Soc. 77, 437–472. https://doi.org/10.1175/1520-0477(1996)077<0437:TNYRP>2.0.CO;2.

Karimi, P., Bastiaanssen, W.G.M., 2015. Spatial evapotranspiration, rainfall and land use data in water accounting; Part 1: Review of the accuracy of the remote sensing data. Hydrol. Earth Syst. Sci. 19, 507–532. https://doi.org/10.5194/hess-19-507-2015.

Keatinge, J.D.H., Breman, H., Manyong, V.M., Vanlauwe, B., Wendt, J., 2001. Sustaining Soil Fertility in West Africa in the Face of Rapidly Increasing Pressure for Agricultural Intensification. In: Sustaining Soil Fertility in West Africa. John Wiley & Sons Ltd, pp. 1–22. https://doi.org/10.2136/sssaspecpub58.ch1.

Khan, M.S., Baik, J., Choi, M., 2020. Inter-comparison of evapotranspiration datasets over heterogeneous landscapes across Australia. Adv. Space Res. 66, 533–545. https://doi.org/10.1016/j.asr.2020.04.037.

B. Koetz W. Bastiaanssen M. Berger P. Defourney U. Del Bello M. Drusch M. Drinkwater R. Duca V. Fernandez D. Ghent R. Guzinski J. Hoogeveen S. Hook J.-P. Lagouarde G. Lemoine I. Manolis P. Martimort J. Masek M. Massart C. Notarnicola T. Udelhoven High Spatio- Temporal Resolution Land Surface Temperature Mission - a Copernicus Candidate Mission in Support of Agricultural Monitoring in: IGARSS 2018–2018 IEEE International Geoscience and Remote Sensing Symposium. Presented at the IGARSS 2018–2018 IEEE International Geoscience and Remote Sensing Symposium 2018 8160 8162 10.1109/IGARSS.2018.8517433.

Koster, R.D., Suarez, M.J., Ducharne, A., Stieglitz, M., Kumar, P., 2000. A catchment-based approach to modeling land surface processes in a general circulation model: 1. Model structure. J. Geophys. Res. Atmos. 105, 24809–24822. https://doi.org/10.1029/2000JD900327.

Krishna, P.R.A., 2019. Evapotranspiration and agriculture-A review. Agric. Rev.

Kuyah, S., Sileshi, G.W., Nkurunziza, L., Chirinda, N., Ndayisaba, P.C., Dimobe, K., Öborn, I., 2021. Innovative agronomic practices for sustainable intensification in sub-Saharan Africa. A Review. Agron. Sustain. Dev. 41, 16. https://doi.org/10.1007/s13593-021-00673-4.

Labedzki, L., 2011. Evapotranspiration. BoD – B. Books on Demand.

Lagouarde, J.-P., Bhattacharya, B.K., Crébassol, P., Gamet, P., Babu, S.S., Boulet, G., Briottet, X., Buddhiraju, K.M., Cherchali, S., Dadou, I., Dedieu, G., Gouhier, M., Hagolle, O., Irvine, M., Jacob, F., Kumar, A., Kumar, K.K., Laignel, B., Mallick, K., Murthy, C.S., Olioso, A., Ottlé, C., Pandya, M.R., Raju, P.V., Roujean, J.-L., Sekhar, M., Shukla, M.V., Singh, S.K., Sobrino, J., Ramakrishnan, R., 2018. The Indian-French Trishna Mission: Earth Observation in the Thermal Infrared with High Spatio-Temporal Resolution, in: IGARSS 2018 - 2018 IEEE International Geoscience and Remote Sensing Symposium. Presented at the IGARSS 2018 - 2018 IEEE International Geoscience and Remote Sensing Symposium, pp. 4078–4081. https://doi.org/10.1109/IGARSS.2018.8518720.

Legates, D.R., McCabe Jr., G.J., 2005. A Re-Evaluation of the Average Annual Global Water Balance. Phys. Geogr. 26, 467–479. https://doi.org/10.2747/0272-3646.26.6.467.

Leuning, R., Zhang, Y.Q., Rajaud, A., Cleugh, H., Tu, K., 2008. A simple surface conductance model to estimate regional evaporation using MODIS leaf area index and the Penman-Monteith equation. Water Resour. Res. 44. https://doi.org/10.1029/2007WR006562.

Li, K.Y., Coe, M.T., Ramankutty, N., Jong, R.D., 2007. Modeling the hydrological impact of land-use change in West Africa. J. Hydrol. 337, 258–268. https://doi.org/10.1016/j.jhydrol.2007.01.038.

Liang, X., Lettenmaier, D.P., Wood, E.F., Burges, S.J., 1994. A simple hydrologically based model of land surface water and energy fluxes for general circulation models. J. Geophys. Res. Atmos. 99, 14415–14428. https://doi.org/10.1029/94JD00483.

Liou, Y.-A., Kar, S.K., 2014. Evapotranspiration Estimation with Remote Sensing and Various Surface Energy Balance Algorithms—A Review. Energies 7, 2821–2849. https://doi.org/10.3390/en7052821.

Lu, J., Wang, G., Chen, T., Li, S., Hagan, D.F.T., Kattel, G., Peng, J., Jiang, T., Su, B., 2021. A harmonized global land evaporation dataset from model-based products covering 1980–2017. Earth Syst. Sci. Data 13, 5879–5898. https://doi.org/10.5194/essd-13-5879-2021.

Maisharou, A., Chirwa, P.W., Larwanou, M., Babalola, F., Ofoegbu, C., 2015. Sustainable land management practices in the Sahel: review of practices, techniques and technologies for land restoration and strategy for up-scaling. Int. For. Rev. 17, 1–19. https://doi.org/10.1505/146554815816006974.

Majozi, N.P., Mannaerts, C.M., Ramoelo, A., Mathieu, R., Mudau, A.E., Verhoef, W., 2017. An Intercomparison of Satellite-Based Daily Evapotranspiration Estimates under Different Eco-Climatic Regions in South Africa. Remote Sens. (Basel) 9, 307. https://doi.org/10.3390/rs9040307.

Marshall, M., Funk, C., Michaelsen, J., 2012. Examining evapotranspiration trends in Africa. Clim. Dyn. 38, 1849–1865. https://doi.org/10.1007/s00382-012-1299-y.

Martens, B., Miralles, D.G., Lievens, H., van der Schalie, R., de Jeu, R.A.M., Fernández-Prieto, D., Beck, H.E., Dorigo, W.A., Verhoest, N.E.C., 2017. GLEAM v3: satellite-based land evaporation and root-zone soil moisture. Geosci. Model Dev. 10, 1903–1925. https://doi.org/10.5194/gmd-10-1903-2017.

McCabe, M.F., Ershadi, A., Jimenez, C., Miralles, D.G., Michel, D., Wood, E.F., 2016. The GEWEX LandFlux project: evaluation of model evaporation using tower-based and globally gridded forcing data. Geosci. Model Dev. 9, 283–305. https://doi.org/10.5194/gmd-9-283-2016.

McCabe, M.F., Wood, E.F., 2006. Scale influences on the remote estimation of evapotranspiration using multiple satellite sensors. Remote Sens. Environ. 105, 271–285. https://doi.org/10.1016/j.rse.2006.07.006.

Melton, F.S., et al., 2022. OpenET: Filling a Critical Data Gap in Water Management for the Western United States. JAWRA Journal of the American Water Resources Association 58, 971–994. https://doi.org/10.1111/1752-1688.12956.

Michel, D., Jiménez, C., Miralles, D.G., Jung, M., Hirschi, M., Ershadi, A., Martens, B., McCabe, M.F., Fisher, J.B., Mu, Q., Seneviratne, S.I., Wood, E.F., Fernández-Prieto, D., 2016. The WACMOS-ET project – Part 1: Tower-scale evaluation of four remote-sensing-based evapotranspiration algorithms. Hydrol. Earth Syst. Sci. 20, 803–822. https://doi.org/10.5194/hess-20-803-2016.

Mira, M., Olioso, A., Gallego-Elvira, B., Courault, D., Garrigues, S., Marloie, O., Hagolle, O., Guillevic, P., Boulet, G., 2016. Uncertainty assessment of surface net radiation derived from Landsat images. Remote Sens. Environ. 175, 251–270. https://doi.org/10.1016/j.rse.2015.12.054.

Miralles, D.G., Gash, J.H., Holmes, T.R., de Jeu, R.A., Dolman, A.J., 2010. Global canopy interception from satellite observations. J. Geophys. Res. Atmos. 115.

Miralles, D.G., Holmes, T.R.H., De Jeu, R.A.M., Gash, J.H., Meesters, A.G.C.A., Dolman, A.J., 2011. Global land-surface evaporation estimated from satellite-based observations. Hydrol. Earth Syst. Sci. 15, 453–469. https://doi.org/10.5194/hess-15-453-2011.

Global Modeling and Assimilation Office (GMAO), 2015. MERRA-2 tavg1_2d_lnd_Nx: 2d,1-Hourly, Time-Averaged, Single-Level, Assimilation, Land Surface Diagnostics V5.12.4, Greenbelt, MD, USA, Goddard Earth Sciences Data and Information Services Center (GES DISC), 10.5067/RKPHT8KC1Y1T.

Molod, A., Takacs, L., Suarez, M., Bacmeister, J., 2015. Development of the GEOS-5 atmospheric general circulation model: evolution from MERRA to MERRA2. Geosci. Model Dev. 8, 1339–1356. https://doi.org/10.5194/gmd-8-1339-2015.

Monteith, J.L., 1965. Evaporation and environment. Symp. Soc. Exp. Biol. 19, 205–234.

Mu, Q., Heinsch, F.A., Zhao, M., Running, S.W., 2007. Development of a global evapotranspiration algorithm based on MODIS and global meteorology data. Remote Sens. Environ. 111, 519–536. https://doi.org/10.1016/j.rse.2007.04.015.

Mu, Q., Zhao, M., Running, S.W., 2011. Improvements to a MODIS global terrestrial evapotranspiration algorithm. Remote Sens. Environ. 115, 1781–1800. https://doi.org/10.1016/j.rse.2011.02.019.

Mueller, B., Hirschi, M., Jimenez, C., Ciais, P., Dirmeyer, P.A., Dolman, A.J., Fisher, J.B., Jung, M., Ludwig, F., Maignan, F., Miralles, D.G., McCabe, M.F., Reichstein, M., Sheffield, J., Wang, K., Wood, E.F., Zhang, Y., Seneviratne, S.I., 2013. Benchmark products for land evapotranspiration: LandFlux-EVAL multi-data set synthesis. Hydrol. Earth Syst. Sci. 17, 3707–3720. https://doi.org/10.5194/hess-17-3707-2013.

Muñoz-Sabater, J., Dutra, E., Agustí-Panareda, A., Albergel, C., Arduini, G., Balsamo, G., Boussetta, S., Choulga, M., Harrigan, S., Hersbach, H., Martens, B., Miralles, D.G., Piles, M., Rodríguez-Fernández, N.J., Zsoter, E., Buontempo, C., Thépaut, J.-N., 2021. ERA5-Land: a state-of-the-art global reanalysis dataset for land applications. Earth Syst. Sci. Data 13, 4349–4383. https://doi.org/10.5194/essd-13-4349-2021.

J. Muñoz-Sabater ERA5-Land hourly data from 2001 to present 2019 https://doi.org/10.24381/CDS.E2161BAC.

Ndiaye, P.M., Bodian, A., Diop, L., Deme, A., Dezetter, A., Djaman, K., Ogilvie, A., 2020. Trend and Sensitivity Analysis of Reference Evapotranspiration in the Senegal River Basin Using NASA Meteorological Data. Water 12, 1957. https://doi.org/10.3390/w12071957.

New, M., Hewitson, B., Stephenson, D.B., Tsiga, A., Kruger, A., Manhique, A., Gomez, B., Coelho, C.A.S., Masisi, D.N., Kululanga, E., Mbambalala, E., Adesina, F., Saleh, H., Kanyanga, J., Adosi, J., Bulane, L., Fortunata, L., Mdoka, M.L., Lajoie, R., 2006. Evidence of trends in daily climate extremes over southern and west Africa. J. Geophys. Res. Atmos. 111. https://doi.org/10.1029/2005JD006289.

Obahoundje, S., Bi, V.H.N., Kouassi, K.L., Ta, M.Y., Amoussou, E., Diedhiou, A., 2020. Validation of Three Satellite Precipitation Products in Two South-Western African Watersheds: Bandama (Ivory Coast) and Mono (Togo). Atmospheric and Climate Sciences 10, 597. https://doi.org/10.4236/acs.2020.104031.

Ollivier, C., Olioso, A., Carrière, S.D., Boulet, G., Chalikakis, K., Chanzy, A., Charlier, J.-B., Combemale, D., Davi, H., Emblanch, C., Marloie, O., Martin-StPaul, N., Mazzilli, N., Simioni, G., Weiss, M., 2021. An evapotranspiration model driven by remote sensing data for assessing groundwater resource in karst watershed. Sci. Total Environ. 781, 146706. https://doi.org/10.1016/j.scitotenv.2021.146706.

Pan, S., Pan, N., Tian, H., Friedlingstein, P., Sitch, S., Shi, H., Arora, V.K., Haverd, V., Jain, A.K., Kato, E., Lienert, S., Lombardozzi, D., Nabel, J.E.M.S., Ottlé, C., Poulter, B., Zaehle, S., Running, S.W., 2020. Evaluation of global terrestrial evapotranspiration using state-of-the-art approaches in remote sensing, machine learning and land surface modeling. Hydrol. Earth Syst. Sci. 24, 1485–1509. https://doi.org/10.5194/hess-24-1485-2020.

Panthou, G., Vischel, T., Lebel, T., 2014. Recent trends in the regime of extreme rainfall in the Central Sahel. Int. J. Climatol. 34, 3998–4006. https://doi.org/10.1002/joc.3984.

Papale, D., Valentini, R., 2003. A new assessment of European forests carbon exchanges by eddy fluxes and artificial neural network spatialization. Glob. Chang. Biol. 9, 525–535. https://doi.org/10.1046/j.1365-2486.2003.00609.x.

Pastorello, G., et al., 2020. The FLUXNET2015 dataset and the ONEFlux processing pipeline for eddy covariance data. Sci. Data 7, 225. https://doi.org/10.1038/s41597-020-0534-3.

Poméon, T., Jackisch, D., Diekkrüger, B., 2017. Evaluating the performance of remotely sensed and reanalysed precipitation data over West Africa using HBV light. J. Hydrol. 547, 222–235. https://doi.org/10.1016/j.jhydrol.2017.01.055.

Priestley, C.H.B., Taylor, R.J., 1972. On the Assessment of Surface Heat Flux and Evaporation Using Large-Scale Parameters. Mon. Weather Rev. 100, 81–92. https://doi.org/10.1175/1520-0493(1972)100<0081:OTAOSH>2.3.CO;2.

Rhoades, C., 1995. Seasonal pattern of nitrogen mineralization and soil moisture beneath Faidherbia albida (synAcacia albida) in central malawi. Agroforest Syst 29, 133–145. https://doi.org/10.1007/BF00704882.

Rienecker, M.M., Suarez, M.J., Gelaro, R., Todling, R., Bacmeister, J., Liu, E., Bosilovich, M.G., Schubert, S.D., Takacs, L., Kim, G.-K., Bloom, S., Chen, J., Collins, D., Conaty, A., da Silva, A., Gu, W., Joiner, J., Koster, R.D., Lucchesi, R., Molod, A., Owens, T., Pawson, S., Pegion, P., Redder, C.R., Reichle, R., Robertson, F. R., Ruddick, A.G., Sienkiewicz, M., Woollen, J., 2011. MERRA: NASA's Modern-Era Retrospective Analysis for Research and Applications. J. Clim. 24, 3624–3648. https://doi.org/10.1175/JCLI-D-11-00015.1.

Rodell, M., Houser, P.R., Jambor, U., Gottschalck, J., Mitchell, K., Meng, C.-J., Arsenault, K., Cosgrove, B., Radakovich, J., Bosilovich, M., Entin, J.K., Walker, J.P., Lohmann, D., Toll, D., 2004. The Global Land Data Assimilation System. Bull. Am. Meteorol. Soc. 85, 381–394. https://doi.org/10.1175/BAMS-85-3-381.

Roudier, P., Ducharne, A., Feyen, L., 2014. Climate change impacts on runoff in West Africa: a review. Hydrol. Earth Syst. Sci. 18, 2789–2801. https://doi.org/10.5194/hess-18-2789-2014.

Roupsard, O., Audebert, A., Ndour, A.P., Clermont-Dauphin, C., Agbohessou, Y., Sanou, J., Koala, J., Faye, E., Sambakhe, D., Jourdan, C., le Maire, G., Tall, L., Sanogo, D., Seghieri, J., Cournac, L., Leroux, L., 2020. How far does the tree affect the crop in agroforestry? New spatial analysis methods in a Faidherbia parkland. Agr Ecosyst Environ 296, 106928. https://doi.org/10.1016/j.agee.2020.106928.

Ryu, Y., Baldocchi, D.D., Kobayashi, H., van Ingen, C., Li, J., Black, T.A., Beringer, J., van Gorsel, E., Knohl, A., Law, B.E., Roupsard, O., 2011. Integration of MODIS land and atmosphere products with a coupled-process model to estimate gross primary productivity and evapotranspiration from 1 km to global scales. Global Biogeochem. Cycles 25. https://doi.org/10.1029/2011GB004053.

Salazar-Martínez, D., Holwerda, F., Holmes, T.R.H., Yépez, E.A., Hain, C.R., Alvarado-Barrientos, S., Ángeles-Pérez, G., Arredondo-Moreno, T., Delgado-Balbuena, J., Figueroa-Espinoza, B., Garatuza-Payán, J., González del Castillo, E., Rodríguez, J.C., Rojas-Robles, N.E., Uuh-Sonda, J.M., Vivoni, E.R., 2022. Evaluation of remote sensing-based evapotranspiration products at low-latitude eddy covariance sites. J. Hydrol. 610, 127786. https://doi.org/10.1016/j.jhydrol.2022.127786.

Satgé, F., Defrance, D., Sultan, B., Bonnet, M.-P., Seyler, F., Rouché, N., Pierron, F., Paturel, J.-E., 2020. Evaluation of 23 gridded precipitation datasets across West Africa. J. Hydrol. 581, 124412. https://doi.org/10.1016/j.jhydrol.2019.124412.

Senay, G.B., Budde, M., Verdin, J.P., Melesse, A.M., 2007. A Coupled Remote Sensing and Simplified Surface Energy Balance Approach to Estimate Actual Evapotranspiration from Irrigated Fields. Sensors 7, 979–1000. https://doi.org/10.3390/s7060979.

Senay, G.B., Bohms, S., Singh, R.K., Gowda, P.H., Velpuri, N.M., Alemu, H., Verdin, J.P., 2013. Operational Evapotranspiration Mapping Using Remote Sensing and Weather Datasets: A New Parameterization for the SSEB Approach. JAWRA Journal of the American Water Resources Association 49, 577–591. https://doi.org/10.1111/jawr.12057.

Senay, G.B., Friedrichs, M., Morton, C., Parrish, G.E.L., Schauer, M., Khand, K., Kagone, S., Boiko, O., Huntington, J., 2022. Mapping actual evapotranspiration using Landsat for the conterminous United States: Google Earth Engine implementation and assessment of the SSEBop model. Remote Sens. Environ. 275, 113011. https://doi.org/10.1016/j.rse.2022.113011.

Siegwart, L., Bertrand, I., Roupsard, O., Jourdan, C., 2023. Contribution of tree and crop roots to soil carbon stocks in a Sub-Sahelian agroforestry parkland in Senegal. Agr Ecosyst Environ 352, 108524. https://doi.org/10.1016/j.agee.2023.108524.

Simonneaux, V., Duchemin, B., Helson, D., Er-Raki, S., Olioso, A., Chehbouni, A.G., 2008. The use of high-resolution image time series for crop classification and evapotranspiration estimate over an irrigated area in central Morocco. Int. J. Remote Sens. 29, 95–116. https://doi.org/10.1080/01431160701250390.

Siriri, D., Wilson, J., Coe, R., Tenywa, M.M., Bekunda, M.A., Ong, C.K., Black, C.R., 2013. Trees improve water storage and reduce soil evaporation in agroforestry systems on bench terraces in SW Uganda. Agroforest Syst 87, 45–58. https://doi.org/10.1007/s10457-012-9520-x.

Su, Z., 2002. The Surface Energy Balance System (SEBS) for estimation of turbulent heat fluxes. Hydrol. Earth Syst. Sci. 6, 85–100. https://doi.org/10.5194/hess-6-85-2002.

Thompson, D.R., Basilio, R., Brosnan, I., Cawse-Nicholson, K., Chadwick, K.D., Guild, L., Gierach, M., Green, R.O., Hook, S., Horner, S.D., Hulley, G., Kokaly, R., Miller, C.E., Miner, K.R., Lee, C., Limonadi, D., Luvall, J., Pavlick, R., Phillips, B., Poulter, B., Raiho, A., Reath, K., Uz, S.S., Sen, A., Serbin, S., Schimel, D., Townsend, P., Turner, W., Turpie, K., Team, T.S., 2022. Ongoing Progress Toward NASA's Surface Biology and Geology Mission, in: IGARSS 2022 - 2022 IEEE International Geoscience and Remote Sensing Symposium. Presented at the IGARSS 2022 - 2022 IEEE International Geoscience and Remote Sensing Symposium, pp. 5007–5010. https://doi.org/10.1109/IGARSS46834.2022.9884123.

Tramontana, G., Jung, M., Schwalm, C.R., Ichii, K., Camps-Valls, G., Ráduly, B., Reichstein, M., Arain, M.A., Cescatti, A., Kiely, G., Merbold, L., Serrano-Ortiz, P., Sickert, S., Wolf, S., Papale, D., 2016. Predicting carbon dioxide and energy fluxes across global FLUXNET sites with regression algorithms. Biogeosciences 13, 4291–4313. https://doi.org/10.5194/bg-13-4291-2016.

Trenberth, K.E., Smith, L., Qian, T., Dai, A., Fasullo, J., 2007. Estimates of the Global Water Budget and Its Annual Cycle Using Observational and Model Data. J. Hydrometeorol. 8, 758–769. https://doi.org/10.1175/JHM600.1.

Tschora, H., Cherubini, F., 2020. Co-benefits and trade-offs of agroforestry for climate change mitigation and other sustainability goals in West Africa. Global Ecol. Conserv. 22, e00919. https://doi.org/10.1016/j.gecco.2020.e00919.

Twine, T.E., Kustas, W.P., Norman, J.M., Cook, D.R., Houser, P.R., Meyers, T.P., Prueger, J.H., Starks, P.J., Wesely, M.L., 2000. Correcting eddy-covariance flux underestimates over a grassland. Agric. For. Meteorol. 103, 279–300. https://doi.org/10.1016/S0168-1923(00)00123-4.

Velluet, C., Demarty, J., Cappelaere, B., Braud, I., Issoufou, H.-B.-A., Boulain, N., Ramier, D., Mainassara, I., Charvet, G., Boucher, M., Chazarin, J.-P., Oï, M., Yahou, H., Maidaji, B., Arpin-Pont, F., Benarrosh, N., Mahamane, A., Nazoumou, Y., Favreau, G., Seghieri, J., 2014. Building a field- and model-based climatology of local water and energy cycles in the cultivated Sahel : annual budgets and seasonality. Hydrol. Earth Syst. Sci. 18, 5001–5024. https://doi.org/10.5194/hess-18-5001-2014.

Velpuri, N.M., Senay, G.B., Singh, R.K., Bohms, S., Verdin, J.P., 2013. A comprehensive evaluation of two MODIS evapotranspiration products over the conterminous United States: Using point and gridded FLUXNET and water balance ET. Remote Sens. Environ. 139, 35–49. https://doi.org/10.1016/j.rse.2013.07.013.

Vincent, A., Inglada, J., Luque, P., 2022. Santiago, Sahel Land Cover OSO 2018. Zenodo.

Vinukollu, R.K., Meynadier, R., Sheffield, J., Wood, E.F., 2011a. Multi-model, multi-sensor estimates of global evapotranspiration: climatology, uncertainties and trends. Hydrol. Process. 25, 3993–4010. https://doi.org/10.1002/hyp.8393.

Vinukollu, R.K., Wood, E.F., Ferguson, C.R., Fisher, J.B., 2011b. Global estimates of evapotranspiration for climate studies using multi-sensor remote sensing data: Evaluation of three process-based approaches. Remote Sens. Environ. 115, 801–823. https://doi.org/10.1016/j.rse.2010.11.006.

Wang, W., Lin, H., Chen, N., Chen, Z., 2021. Evaluation of multi-source precipitation products over the Yangtze River Basin. Atmos. Res. 249, 105287. https://doi.org/10.1016/j.atmosres.2020.105287.

Wanniarachchi, S., Sarukkalige, R., 2022. A Review on Evapotranspiration Estimation in Agricultural Water Management: Past, Present, and Future. Hydrology 9, 123. https://doi.org/10.3390/hydrology9070123.

WaPOR database methodology, 2020. FAO. https://doi.org/10.4060/ca9894en.

Weerasinghe, I., Bastiaanssen, W., Mul, M., Jia, L., van Griensven, A., 2020. Can we trust remote sensing evapotranspiration products over Africa? Hydrol. Earth Syst. Sci. 24, 1565–1586. https://doi.org/10.5194/hess-24-1565-2020.

Wutzler, T., Lucas-Moffat, A., Migliavacca, M., Knauer, J., Sickel, K., Šigut, L., Menzer, O., Reichstein, M., 2018. Basic and extensible post-processing of eddy covariance flux data with REddyProc. Biogeosciences 15, 5015–5030. https://doi.org/10.5194/bg-15-5015-2018.

Yang, Y., Guan, H., Long, D., Liu, B., Qin, G., Qin, J., Batelaan, O., 2015. Estimation of Surface Soil Moisture from Thermal Infrared Remote Sensing Using an Improved Trapezoid Method. Remote Sens. (Basel) 7, 8250–8270. https://doi.org/10.3390/rs70708250.

Yang, F., Ichii, K., White, M.A., Hashimoto, H., Michaelis, A.R., Votava, P., Zhu, A.-X., Huete, A., Running, S.W., Nemani, R.R., 2007. Developing a continental-scale measure of gross primary production by combining MODIS and AmeriFlux data through Support Vector Machine approach. Remote Sens. Environ. 110, 109–122. https://doi.org/10.1016/j.rse.2007.02.016.

Yuan, W., Liu, S., Yu, G., Bonnefond, J.-M., Chen, J., Davis, K., Desai, A.R., Goldstein, A. H., Gianelle, D., Rossi, F., Suyker, A.E., Verma, S.B., 2010. Global estimates of evapotranspiration and gross primary production based on MODIS and global meteorology data. Remote Sens. Environ. 114, 1416–1431. https://doi.org/10.1016/j.rse.2010.01.022.

Zhang, Y., Leuning, R., Hutley, L.B., Beringer, J., McHugh, I., Walker, J.P., 2010. Using long-term water balances to parameterize surface conductances and calculate evaporation at 0.05° spatial resolution. Water Resources Research 46. https://doi.org/10.1029/2009WR008716.

Zhang, K., Kimball, J.S., Nemani, R.R., Running, S.W., Hong, Y., Gourley, J.J., Yu, Z., 2015. Vegetation Greening and Climate Change Promote Multidecadal Rises of Global Land Evapotranspiration. Sci. Rep. 5, 15956. https://doi.org/10.1038/srep15956.

Zhang, K., Kimball, J.S., Running, S.W., 2016a. A review of remote sensing based actual evapotranspiration estimation. WIREs Water 3, 834–853. https://doi.org/10.1002/wat2.1168.

Zhang, X., Liang, S., Wang, G., Yao, Y., Jiang, B., Cheng, J., 2016b. Evaluation of the Reanalysis Surface Incident Shortwave Radiation Products from NCEP, ECMWF, GSFC, and JMA Using Satellite and Surface Observations. Remote Sens. (Basel) 8, 225. https://doi.org/10.3390/rs8030225.

Zhang, Y., Peña-Arancibia, J.L., McVicar, T.R., Chiew, F.H.S., Vaze, J., Liu, C., Lu, X., Zheng, H., Wang, Y., Liu, Y.Y., Miralles, D.G., Pan, M., 2016c. Multi-decadal trends in global terrestrial evapotranspiration and its components. Sci. Rep. 6, 19124. https://doi.org/10.1038/srep19124.

Zhang, Y., Pan, M., Sheffield, J., Siemann, A.L., Fisher, C.K., Liang, M., Beck, H.E., Wanders, N., MacCracken, R.F., Houser, P.R., Zhou, T., Lettenmaier, D.P., Pinker, R. T., Bytheway, J., Kummerow, C.D., Wood, E.F., 2018. A Climate Data Record (CDR) for the global terrestrial water budget: 1984–2010. Hydrol. Earth Syst. Sci. 22, 241–263. https://doi.org/10.5194/hess-22-241-2018.

Zhang, Y., Kong, D., Gan, R., Chiew, F.H.S., McVicar, T.R., Zhang, Q., Yang, Y., 2019. Coupled estimation of 500 m and 8-day resolution global evapotranspiration and gross primary production in 2002–2017. Remote Sens. Environ. 222, 165–182. https://doi.org/10.1016/j.rse.2018.12.031.

Zhao, M., Heinsch, F.A., Nemani, R.R., Running, S.W., 2005. Improvements of the MODIS terrestrial gross and net primary production global data set. Remote Sens. Environ. 95, 164–176. https://doi.org/10.1016/j.rse.2004.12.011.

Zhuang, Q., Shi, Y., Shao, H., Zhao, G., Chen, D., 2021. Evaluating the SSEBop and RSPMPT Models for Irrigated Fields Daily Evapotranspiration Mapping with MODIS and CMADS Data. Agriculture 11, 424. https://doi.org/10.3390/agriculture11050424.